Neuroprosthetics - Exercise 1

Alexander Koenig

16. November 2019

1 Signal Generation

A superposition of signals can be calculated with equation 1 where A_o is the signal offset, and A_i is the amplitude of the frequency component F_i.

$$f(t) = A_o + \sum_{i=1}^{n} A_i \cdot \sin(2\pi F_i \cdot t) \tag{1}$$

Figure 1 shows the superposition of three signals with the below properties and an offset A_o of 3. The signal was created with equation 1 and a sampling rate of 100kHz.

i	A_i	F_i
1	1	100 Hz
2	1.5	600 Hz
3	2	9 kHz

2 Single Sided Spectrum

Figure 2 shows the reconstructed single-sided amplitude spectra of the previously presented superimposed signal with different sample rates. The single-sided spectra were calculated by using NumPy's implementation of the Fast Fourier Transformation (FFT). It becomes clear that for a sample rate of 100kHz and 20kHz the underlying frequencies of the signal can be correctly reconstructed. However, this is not the case for the sampling rate of 10kHz as a frequency bin at 1kHz can be observed although it does not correspond to a base frequency.

In signal processing, this phenomenon is called aliasing. Aliasing effects occur if the analyzed signal contains frequencies that are higher than half of the sampling rate. Mathematically, this is expressed by the Nyquist-Shannon sampling theorem (equation 3). The corresponding threshold is called the Nyquist frequency (equation 2).

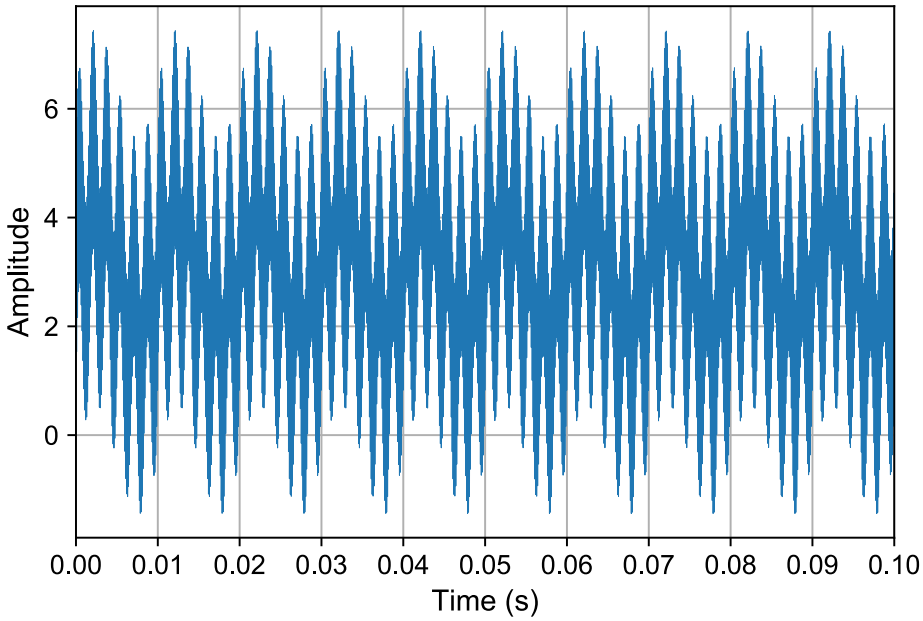

Figure 1: First 100ms of superimposed signal

$$f_{nyquist} = \frac{1}{2} \cdot f_{sampling} \tag{2}$$

$$f_{signal} < f_{nyquist} \tag{3}$$

In the described case the Nyquist frequency is $f_{nyquist} = \frac{1}{2} \cdot 10\text{kHz} = 5\text{kHz}$. This in turn means that to fully reconstruct the signal it must not contain any frequencies greater or equal to 5kHz. However, since the base frequency $F_3 = 9\text{kHz}$ is greater than the Nyquist frequency, the signal cannot be correctly reconstructed and aliasing effects occur. To prevent aliasing a low-pass filter can be applied to the signal before the calculation of the spectrum.

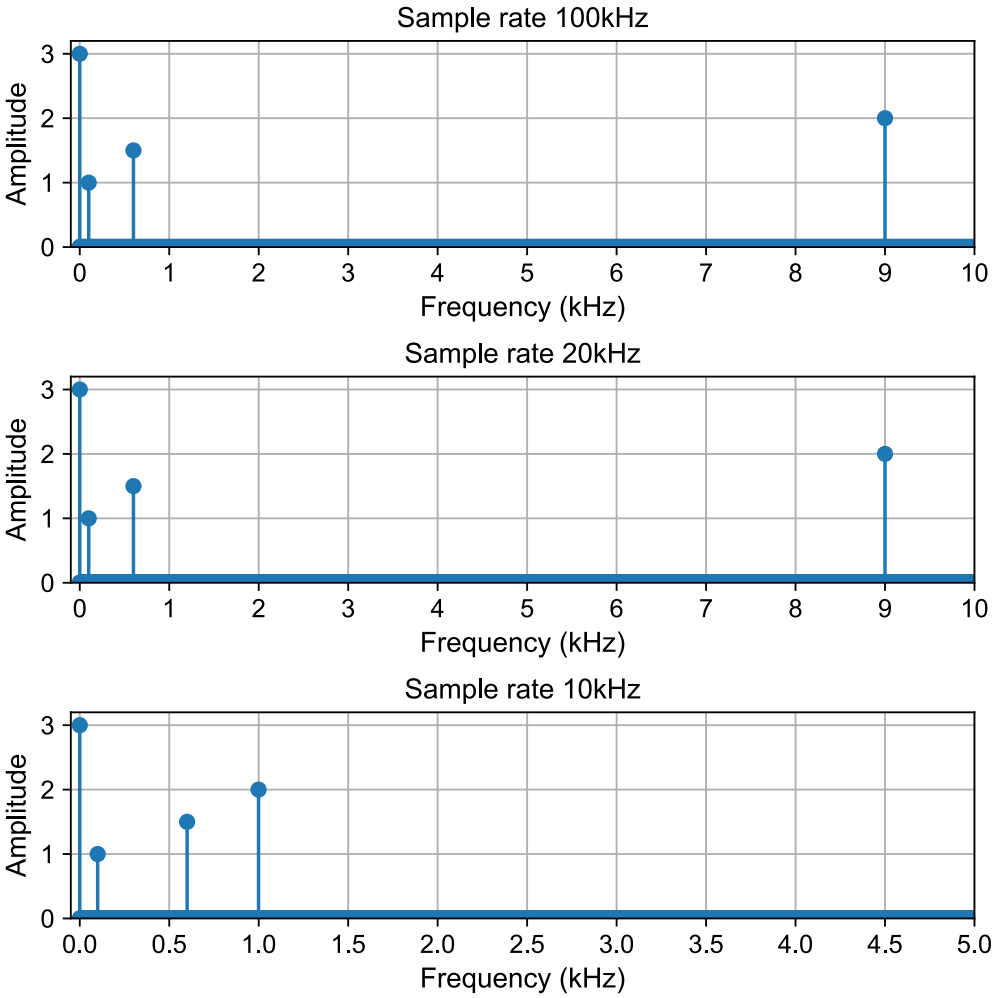

Figure 2: Single sided amplitude spectra for different sample rates

Neuroprosthetics - Exercise 2

Alexander Koenig

24. November 2019

1 Plot Slope Fields and Isoclines

Figures 1 and 2 show the slope fields and isoclines for the ordinary differential equations (ODE) 1 and 2 respectively. An isocline is a line at which the slope (here $\frac{dV}{dt}$) equals to a constant k. The isoclines for the set of constants $K = \{-2, -1, 0, 1, 2\}$ are plotted.

$$\frac{dV}{dt} = 1 - V - t \tag{1}$$

$$\frac{dV}{dt} = sin(t) - \frac{1}{1.5}V \tag{2}$$

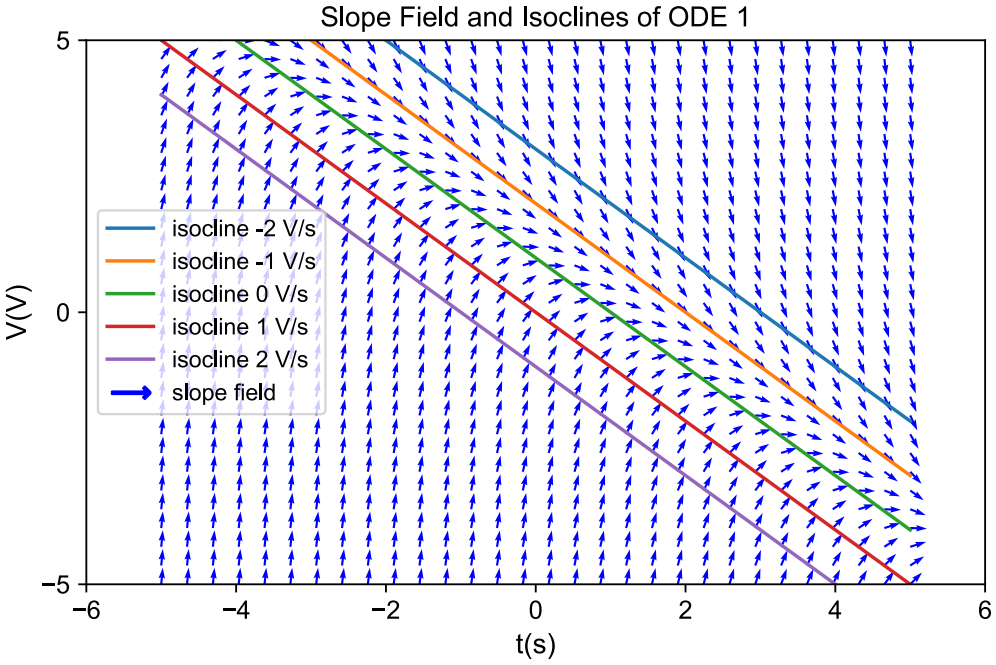

Figure 1: Slope field and isoclines of ODE 1

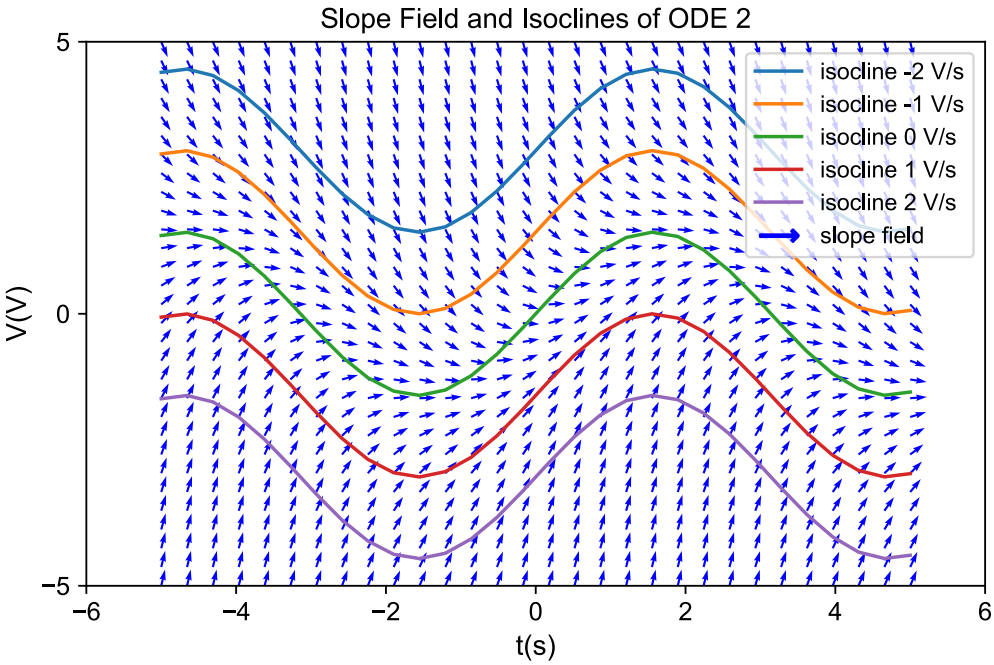

Figure 2: Slope field and isoclines of ODE 2

2 Differential Equations of a Simple Cell Model

The differential equation of the leaky integrate and fire neuron model can be derived from Kirchhoffs law as shown in equation 3. The external current is known and defined by equation 4. The expression for the current through the resistor I_r in equation 5 can simply be derived from Ohm's law $R = \frac{V}{I}$. Furthermore, the capacitor's displacement current in equation 6 can be derived from the relations $I = \frac{dQ}{dt}$ and $Q = C \cdot V$.

$$I_{ex}(t) = I_r(t) + I_c(t) \tag{3}$$

$$I_{ex}(t) = I_{max} \cdot sin(t) \tag{4}$$

$$I_r(t) = \frac{V_r(t)}{R_l} \tag{5}$$

$$I_c(t) = C_m \cdot \frac{dV}{dt} \tag{6}$$

By plugging the results for the components' currents in the original formula 3 we get equation 7 and by rearranging we obtain the final governing differential equation 8. The exercise asks to include another constant term D to the current part of the differential equation, which is done in equation 9.

$$I_{max} \cdot sin(t) = \frac{V_r(t)}{R_l} + C_m \cdot \frac{dV}{dt} \tag{7}$$

$$\frac{dV}{dt} = \frac{1}{C_m}\left(I_{max} \cdot sin(t) - \frac{V_r(t)}{R_l}\right) \tag{8}$$

$$\frac{dV}{dt} = \frac{1}{C_m}\left(I_{max} \cdot sin(t) + D - \frac{V_r(t)}{R_l}\right) \tag{9}$$

Finally, plots of this ordinary differential equation are presented. There are four plots with the following parameters.

R	C_m	I_{max}	D	Plot
1.3Ω	0.8F	0A	0A	A
1.3Ω	0.8F	1A	0A	B
1.3Ω	0.8F	0A	2A	C
1.3Ω	0.8F	1A	2A	D

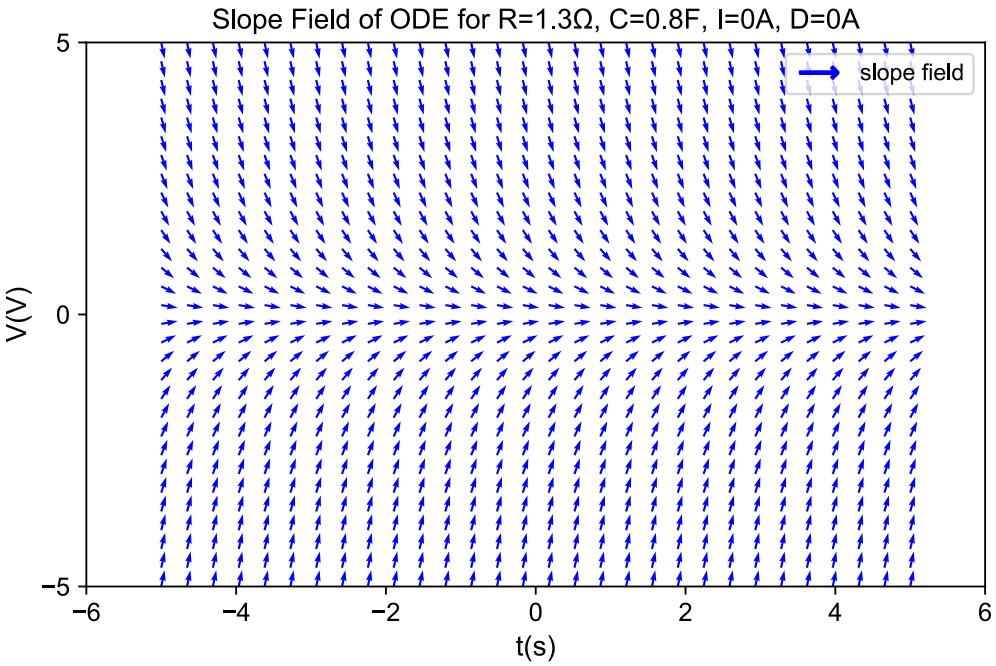

Figure 3: Plot A

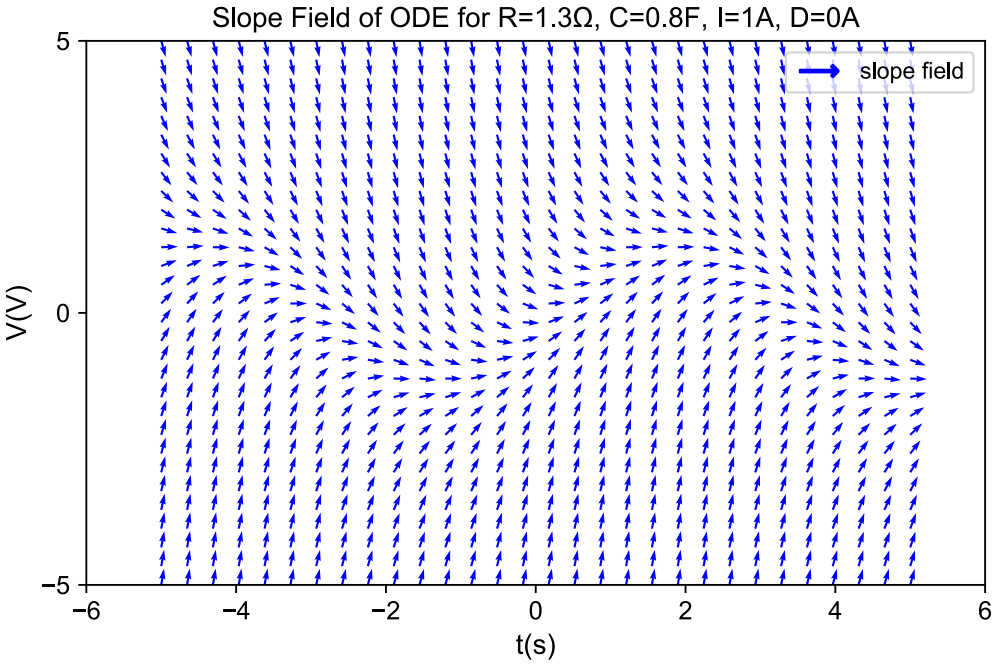

Figure 4: Plot B

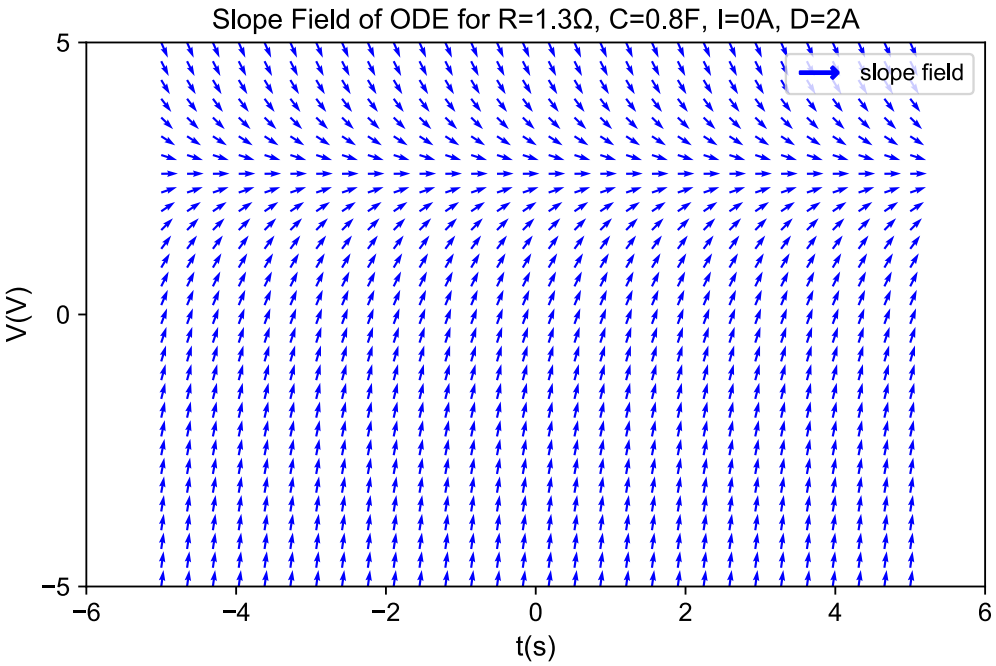

Figure 5: Plot C

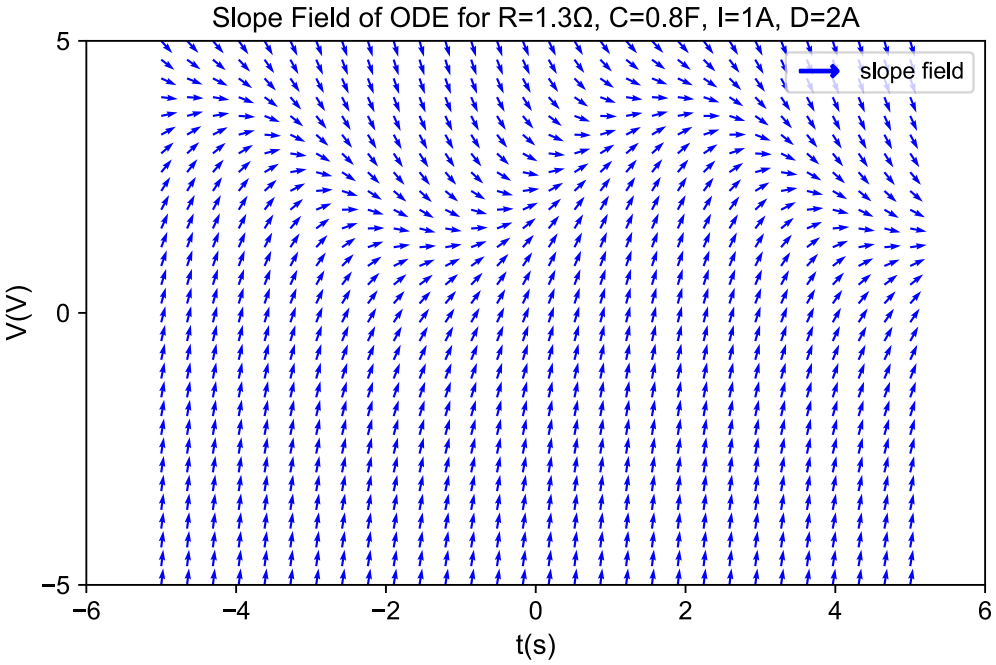

Figure 6: Plot D

Neuroprosthetics - Exercise 3

Alexander Koenig

30. November 2019

1 Solver Implementation

An initial value problem (IVP) $\frac{dV}{dt} = f(V,t)$ with a given $V(t_0) = V_0$ may be solved numerically using a variety of methods. The following numerical solvers for differential equations were implemented in Python. Starting from a given initial value V_0 the next value V_{n+1} can be calculated using the following formulae.

Explicit Euler Method

$$V_{n+1} = V_n + f(V_n, t_n) \cdot \Delta t \tag{1}$$

Heun's Method

$$A = f(V_n, t_n) \tag{2}$$
$$B = f(V_n + A \cdot \Delta t, t_{n+1}) \tag{3}$$
$$V_{n+1} = V_n + \frac{A+B}{2} \cdot \Delta t \tag{4}$$

Equations of the form $\frac{dV}{dt} = A(t)V(t) + B(V,t)$ may be solved with exponential methods such as the Exponential Euler Method.

Exponential Euler Method

$$V_{n+1} = V_n e^{A(t_n)\cdot\Delta t} + \frac{B(V_n, t_n)}{A(t_n)}(e^{A(t_n)\cdot\Delta t} - 1) \tag{5}$$

2 Solve Functions

The initial value problem in equation 6 is solved with the above methods in the interval $t \in [-4.5s, 5s]$ with varying step sizes. It becomes obvious from the plots (figure 1, 2 and 3) that reducing the step size of the respective numerical integration scheme from $1s$ to $0.012s$ yields a more accurate result. However, smaller step sizes come at a computational cost, as more calculations have to be executed. Therefore using an infinitesimal step size is not computationally feasible.

$$\begin{aligned} \frac{dV}{dt} &= 1 - V - t \\ V(t = -4.5) &= V_0 = -4 \end{aligned} \tag{6}$$

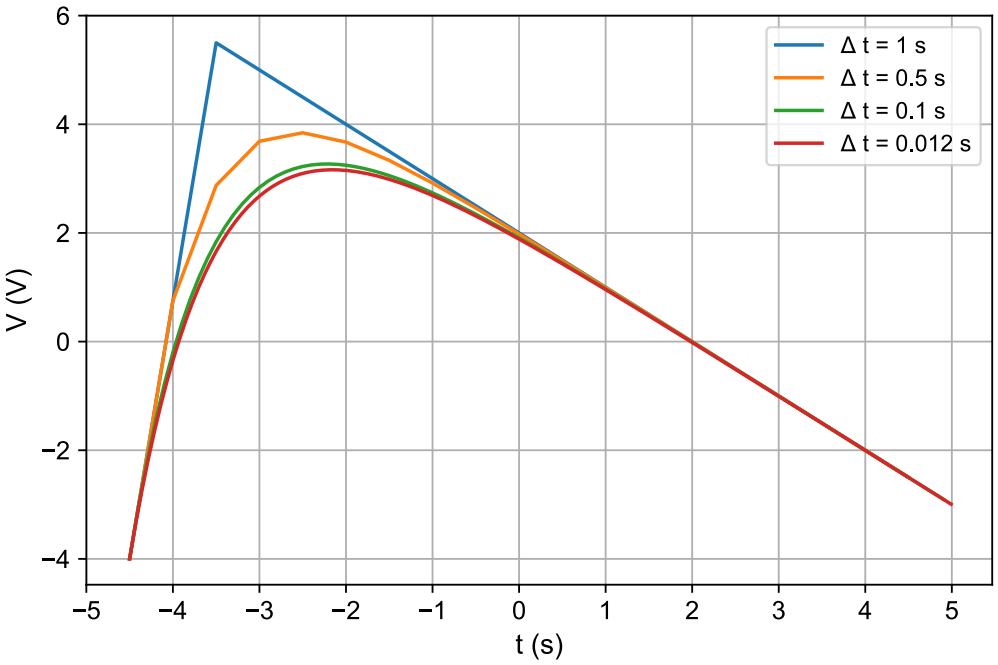

Figure 1: Numerical solution using Explicit Euler

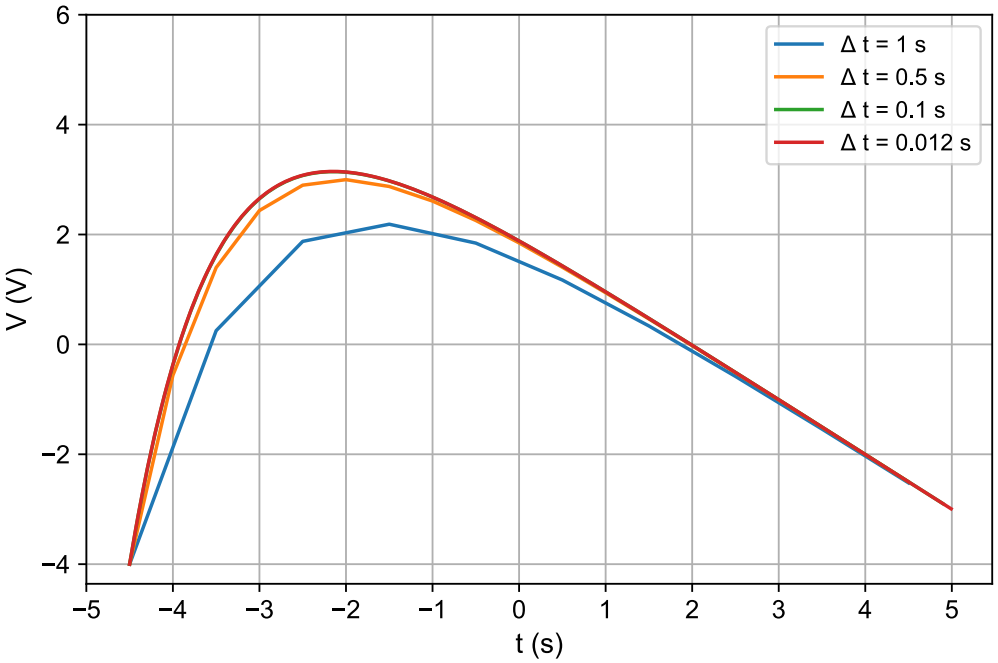

Figure 2: Numerical solution using Heun

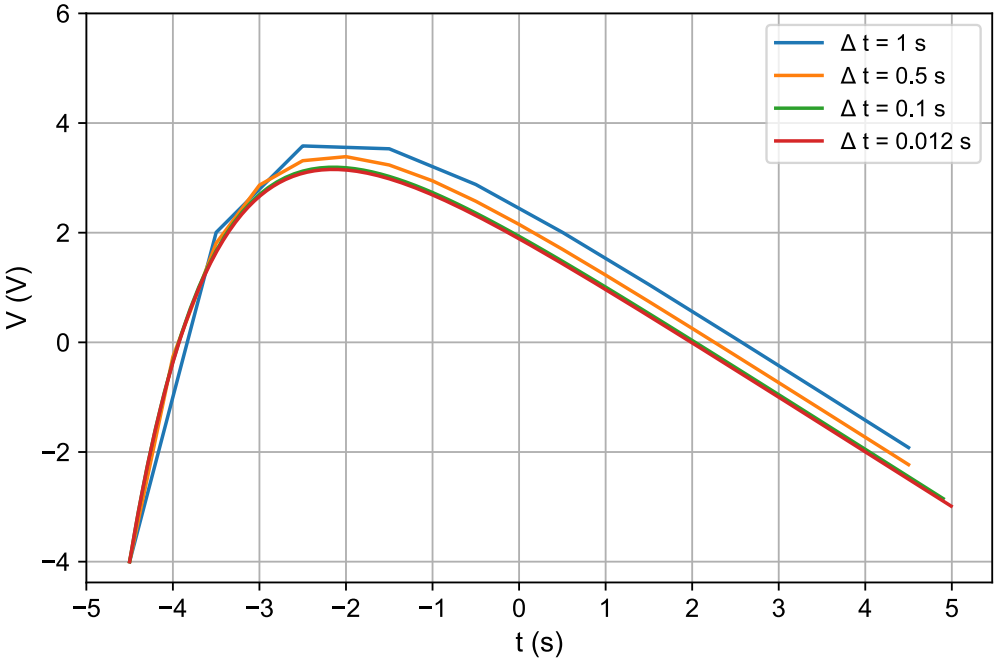

Figure 3: Numerical solution using Exponential Euler

3 The Leaky Integrate and Fire Neuron

The cell membrane voltage of the Leaky Integrate and Fire (LIF) Neuron can be modeled with equation 7. In this example, the external current I_{ex} that stimulates the neuron is either modeled as a constant current ($10\mu A$ and $20\mu A$) or a rectified sine wave (50Hz with $10\mu A$ and $20\mu A$ amplitude). The rectified sine waves are displayed in figure 4.

$$V_{n+1} = \begin{cases} V_n + \frac{\Delta t}{C_m}\left(-g_{leak}\left(V_n - V_{rest}\right) + I_{ex}\left(t_n\right)\right) & V_n < V_{thr} \\ V_{spike} & V_{thr} \leq V_n < V_{spike} \\ V_{rest} & V_{spike} \leq V_n \end{cases} \tag{7}$$

with

- V_n: cell membrane voltage
- $C_m = 1\mu F$: membrane capacitance
- $g_{leak} = 100\mu S$: leak conductivity
- $V_{rest} = -60mV$: cell membrane resting voltage
- $V_{thr} = -20mV$: cell membrane spiking threshold voltage
- $V_{spike} = 20mV$: spiking voltage

The model in equation 7 describes the process of charging and discharging a capacitor with an input current through a resistor. When a constant current is applied to the neuron (see figure 5) the cell membrane voltage of the LIF neuron exponentially increases until a certain threshold voltage is reached. When the threshold is reached the voltage spikes and an action potential occurs. After the spike, the transmembrane potential reaches the resting potential and the process is repeated at a constant rate. Notably, the constant input current is directly proportional to the frequency of charge and discharge cycles.

For the rectified sine input current the process is very similar in that there is still a repeated cycle of charge and discharge of the capacitor (see figure 6). The main difference is that the charging process of the capacitor now follows a different profile. In some cases, the charge from the capacitor can flow back before the threshold is reached and hence a curved transmembrane potential can be observed in these time intervals. Further the rate at which the neuron fires is not constant for the rectified sine input current.

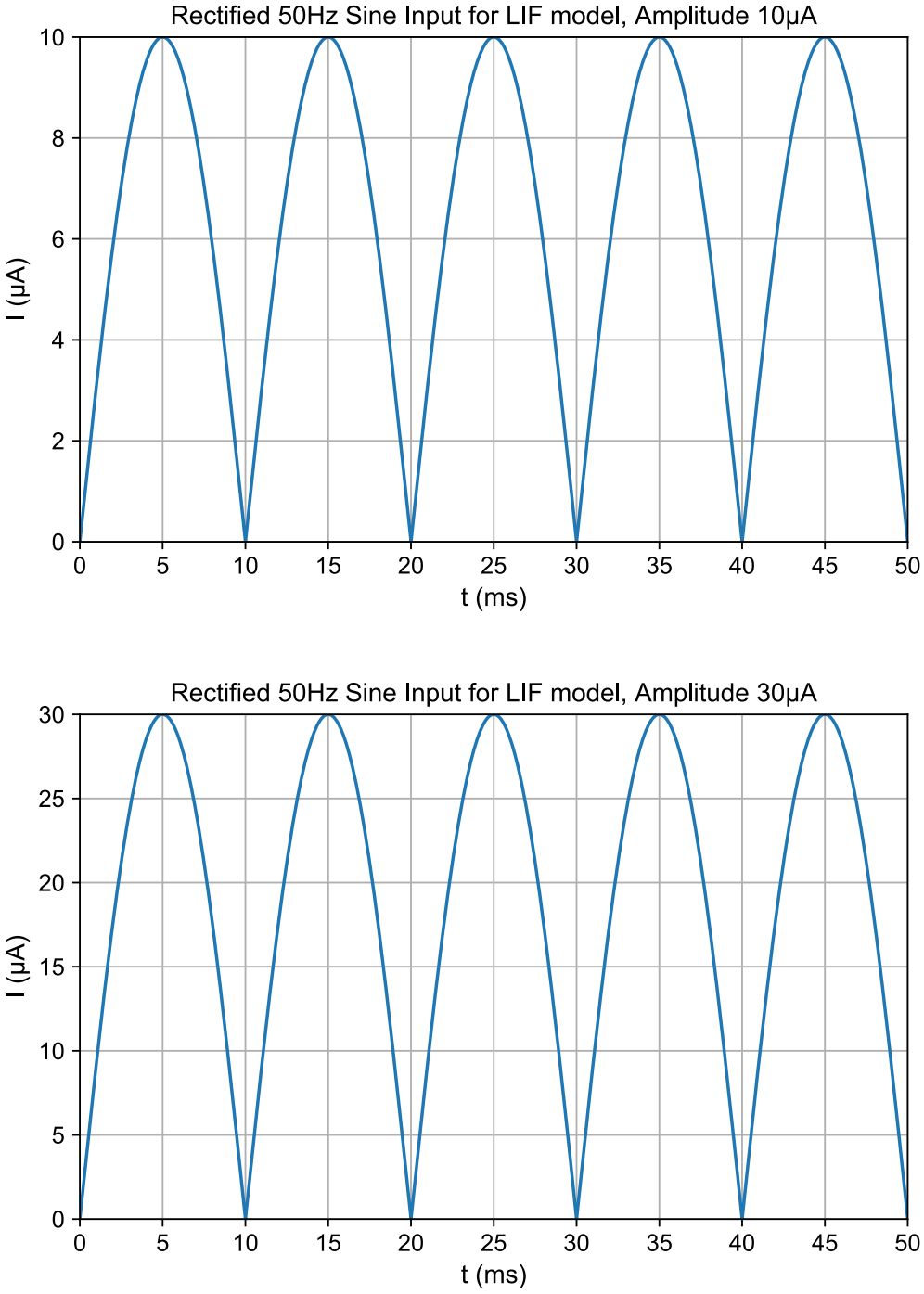

Figure 4: Input currents

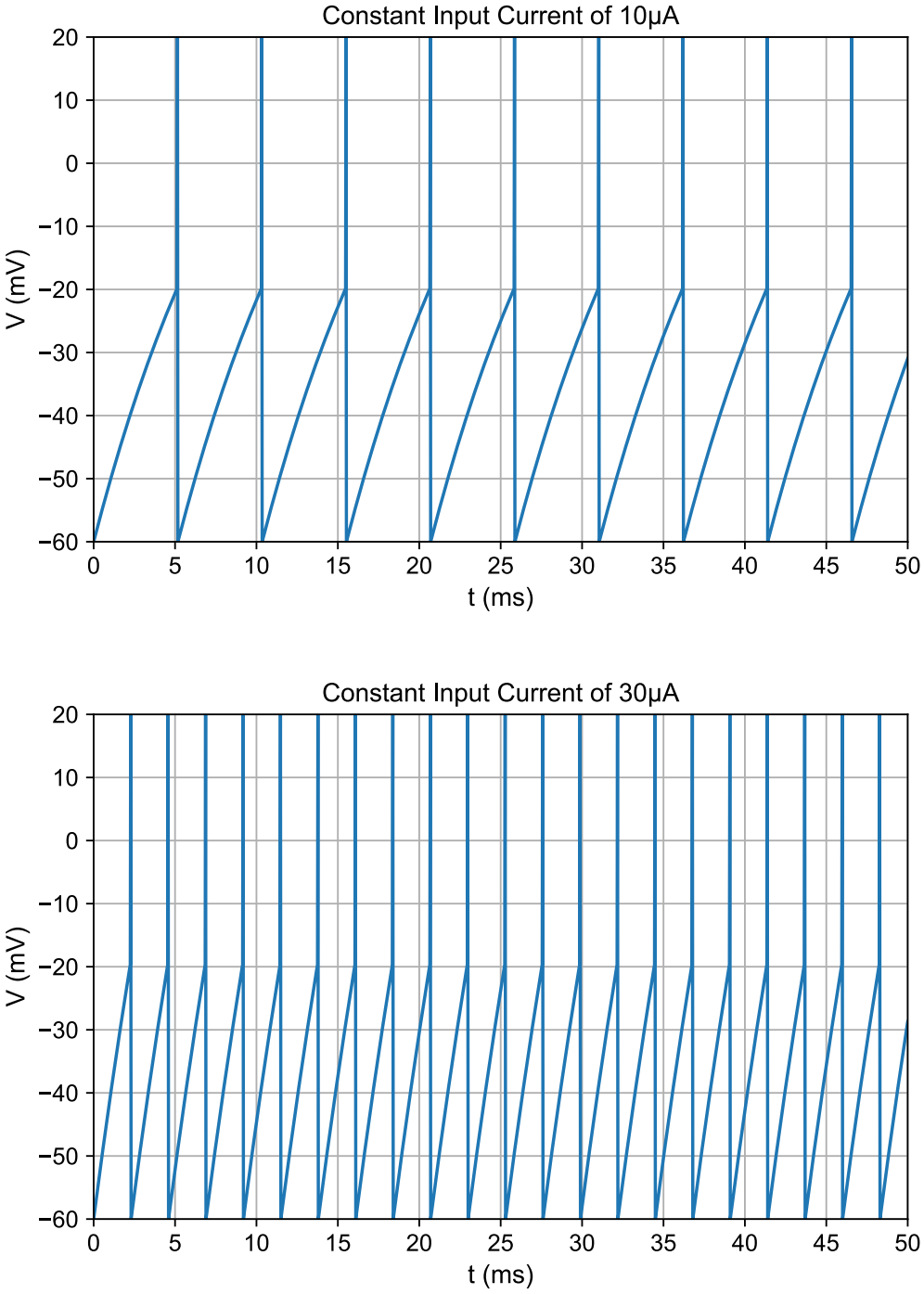

Figure 5: Membrane voltage with constant input current

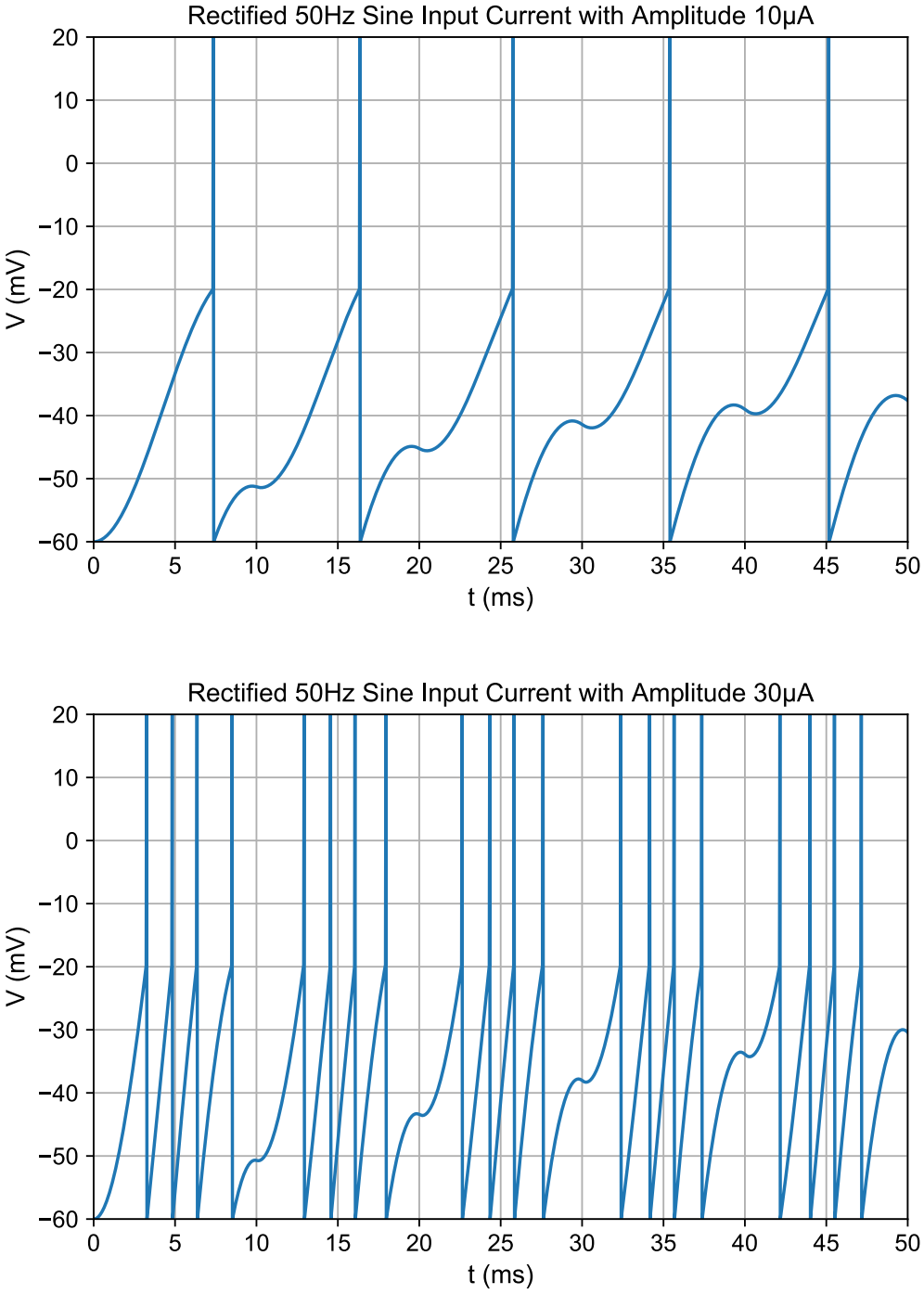

Figure 6: Membrane voltage with rectified sine input current

Neuroprosthetics - Exercise 4

Alexander Koenig

4. December 2019

1 Time Constants and Steady-State Values

Derivation of Formulae

The relationship between the voltage dependent rates α_x, β_x and the time constant τ_x (equation 6) and steady state value x_∞ (equation 7) with $x \in \{m, n, h\}$ can be derived from the gating equation in equation 1.

$$\frac{dx}{dt} = [\alpha_x(1-x) - \beta_x x] \cdot k \tag{1}$$

$$\frac{dx}{dt} = [\alpha_x - \alpha_x x - \beta_x x] \cdot k \tag{2}$$

$$\frac{dx}{dt} = [\alpha_x - (\alpha_x + \beta_x) \cdot x] \cdot k \tag{3}$$

$$\frac{dx}{dt} = (\frac{\alpha_x}{\alpha_x + \beta_x} - x) \cdot (\alpha_x + \beta_x) \cdot k \tag{4}$$

$$\frac{dx}{dt} = \frac{1}{\tau_x}(x_\infty - x) \tag{5}$$

with

$$\tau_x = \frac{1}{(\alpha_x + \beta_x) \cdot k} \tag{6}$$

$$x_\infty = \frac{\alpha_x}{\alpha_x + \beta_x} \tag{7}$$

and the temperature correction factor

$$k = 3^{0.1(T-6.3)} \tag{8}$$

Interpretations of Plots

Figures 1 and 2 show the relationship between the membrane potential and the time constants τ_x. The time constants represent the time needed for the gates to approach their steady state values x_∞ at a specific membrane potential. The steady state values are approached exponentially (see definition of α_x and β_x in section 2).

When figures 1 and 2 are compared a temperature dependency becomes evident. At higher temperatures, the time constants τ_x are shorter for all membrane potentials and hence the steady-state values x_∞ are approached sooner. Vice versa, it takes longer to approach the steady-state values of the gating variables if the temperature is lower. This is because the temperature is inversely proportional to the time constant which is evident from equations 6 and 8.

It is clear that the m gate (sodium activation gate) has the smallest time constants and hence can approach its steady-state value the fastest. This corresponds to the well-known fact that sodium channels are very quick to activate and deactivate. It takes the n gate (potassium activation gate) longer to approach the steady-state value than the m gate. The h gate (sodium inactivation gate) is the slowest of all gates at resting potential ($\mathrm{V} = 0\mathrm{mV} \pm 15\mathrm{mV}$). However, for higher or lower membrane potentials the h gate is faster than the n gate but still slower than the m gate. These observations are valid for both temperatures.

Figures 3 and 4 show the relationships between the membrane potential and the steady state values for the gating variables at different temperatures. Since x_∞ is not temperature dependent both plots are identical. Note that equations 14 and 15 model the sodium and potassium channels respectively.

For strongly negative membrane potentials the sodium inactivation gate is fully opened ($P_{open} \approx 1$) but both sodium and potassium activation gates are closed ($P_{open} \approx 0$). Hence no sodium or potassium current can flow (refer to equations 14 and 15). At resting potential ($V_{rest} = 0$) the sodium channels are nearly completely closed ($m_\infty = 0.05$ and $h_\infty = 0.60$) while a few potassium channels are open ($n_\infty = 0.32$). When the cell begins to depolarize and the membrane potential rises, more sodium and potassium channels open. The sodium channels open faster than the potassium channels because τ_m is much smaller than τ_n. As observed earlier the sodium inactivation gates are especially slow in the region of the resting potential and hence the depolarization can continue - an action potential occurs. When the membrane potential rises further the sodium and potassium activation gates are fully opened ($P_{open} \approx 1$) whereas the sodium inactivation gate is fully closed ($P_{open} \approx 0$). As a result, no further inflow of sodium ions is possible, but potassium ions can still flow out of the cell. The cell repolarizes and both ion channels start to close. Because the potassium channels close slower than the sodium channels even more potassium ions can flow out of the cell. The cell enters the hyperpolarization phase before it recovers back to the resting potential.

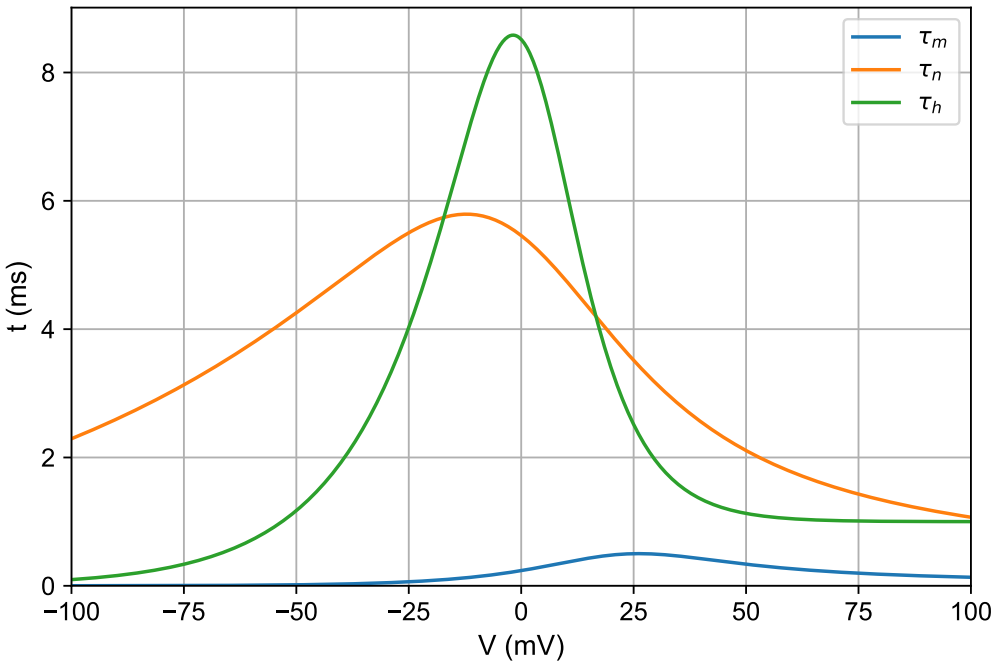

Figure 1: Time constants for temperature 6.3 °C

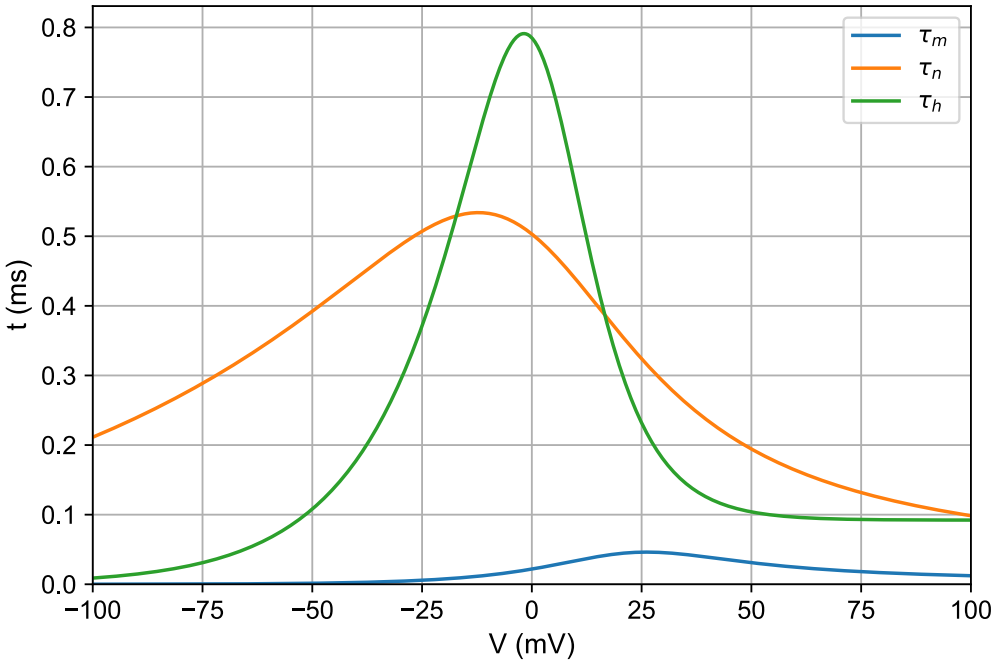

Figure 2: Time constants for temperature 28 °C

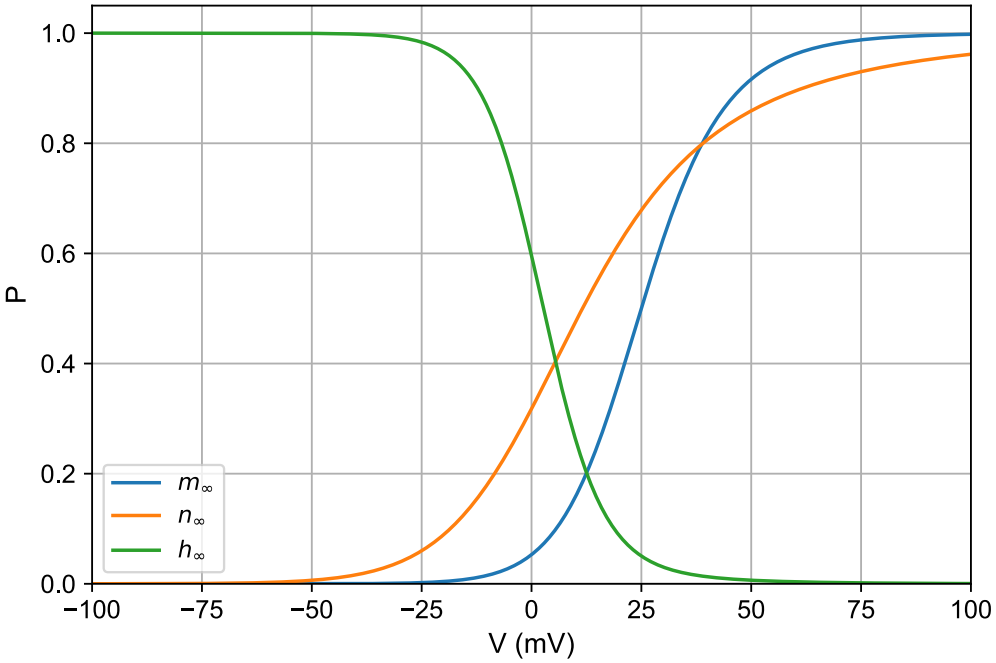

Figure 3: Steady state values for temperature 6.3 °C

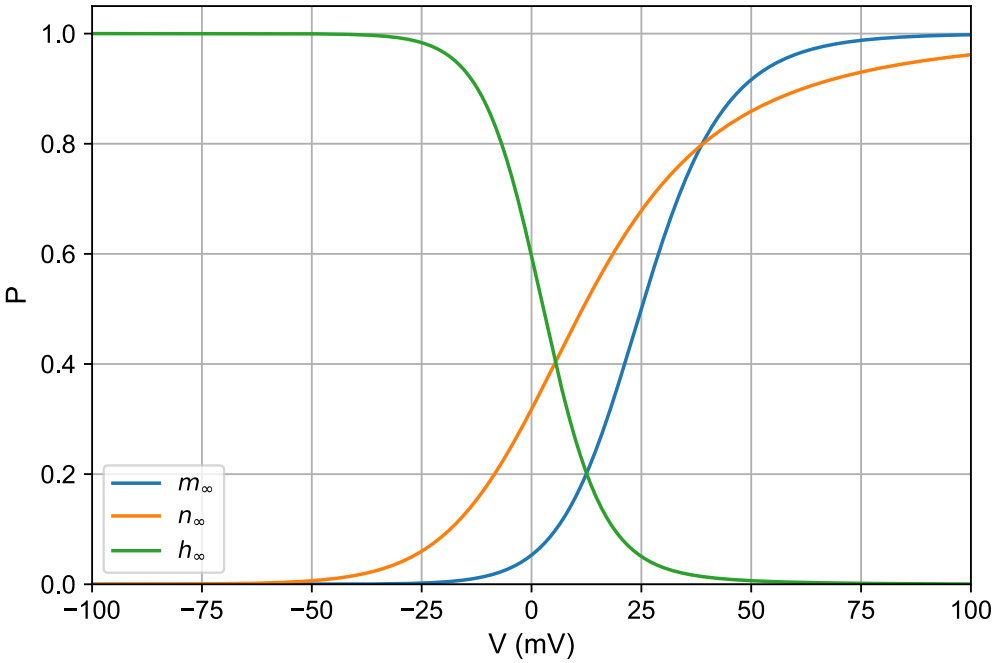

Figure 4: Steady state values for temperature 28 °C

2 Hodgkin-Huxley Neuron Model

By conducting voltage-clamp experiments to investigate the squid giant axon Hodgkin and Huxley formulated a mathematical model that describes the formation and propagation of action potentials. The model is governed by four nonlinear differential equations that represent the electrical characteristics of excitable cells. Equation 9 models the potential across the cell membrane and equations 10, 11 and 12 describe the behaviour of the gating variables. All constants and units are used as in the original publication by Hodgkin and Huxley.

$$\frac{dV}{dt} = \frac{1}{c}\left(-i_{ion} + i_{stimulus}\right) \tag{9}$$

$$\frac{dm}{dt} = \left[\alpha_m(1-m) - \beta_m m\right] k \tag{10}$$

$$\frac{dn}{dt} = \left[\alpha_n(1-n) - \beta_n n\right] k \tag{11}$$

$$\frac{dh}{dt} = \left[\alpha_h(1-h) - \beta_h h\right] k \tag{12}$$

with the ion currents

$$i_{ion} = i_{Na} + i_K + i_L \tag{13}$$

$$i_{Na} = \bar{g}_{Na} m^3 h \left(V - V_{Na}\right) \tag{14}$$

$$i_K = \bar{g}_K n^4 \left(V - V_K\right) \tag{15}$$

$$i_L = \bar{g}_L \left(V - V_L\right) \tag{16}$$

and the rate equations

$$\alpha_m = \frac{2.5 - 0.1V}{e^{(2.5-0.1V)} - 1} \tag{17}$$

$$\alpha_n = \frac{0.1 - 0.01V}{e^{(1-0.1V)} - 1} \tag{18}$$

$$\alpha_h = 0.07e^{-V/20} \tag{19}$$

$$\beta_m = 4e^{-V/18} \tag{20}$$

$$\beta_n = 0.125e^{-V/80} \tag{21}$$

$$\beta_h = \frac{1}{e^{(3-0.1V)} + 1} \tag{22}$$

In this exercise the stimulating current $i_{stimulus}$ consists of five 5ms long rectangular pulses with a gap of 10ms and the amplitudes 1μA, 2μA, 3μA, 4μA, 5μA for 6.3 °C and 2μA, 4μA, 8μA, 16μA, 32μA for 28 °C respectively. The stimulating currents are displayed in figures 5 and 6.

Difference between Temperatures

Membrane Potential: The amplitude of the spikes in figure 7 is larger than in figure 8 even though the stimulation current is higher. We conclude from this that higher stimulation currents are needed at higher temperatures to generate an action potential. This is due to the more rapid opening and closing of ion channels at higher temperatures. Another observation that relates to this is that each stimulus leads to exactly one action potential in figure 7 whereas one stimulus can produce multiple spikes in figure 8. Hence the membrane potential spikes in a more regular pattern for the lower temperature.

Gating Variables: The gating variables tend towards their steady state values ($m_\infty = 0.05$, $h_\infty = 0.60$, $n_\infty = 0.32$) faster at higher temperatures. As a result more action potentials can be released with one stimulus. At the higher temperature the gates are also more responsive to the stimuli that do not elicit an action potential (i.e. at $t \in \{0ms, 5ms\}$, $t \in \{15ms, 20ms\}$ and $t \in \{30ms, 35ms\}$).

Ion Currents: The amplitude of the potassium and sodium currents is slightly reduced by the temperature increase. The current spikes correspond to the action potentials (with the sodium current rising slightly earlier than the potassium current as the sodium gates open quicker). The sodium currents are negative (cations flow into the cell) whereas the potassium currents are positive (cations flow out of the cell).

Generation of an Action Potential

An action potential is a large spike in the membrane potential of a neuron. The generation of action potentials is best explained by investigating the behavior of the gating variables for sodium and potassium in figure 9.

A stimulation current of 1 μA and 2 μA slightly rises the membrane potential in the interval $t \in \{0ms, 5ms\}$ and $t \in \{15ms, 20ms\}$ but is not sufficient to overcome the threshold voltage (see figure 7). However, a stimulus of 3 μA in the interval $t \in \{30ms, 35ms\}$ is sufficient to overcome this threshold, which activates both sodium and potassium channels through the m and n gates. But the sodium channels m open much faster than the potassium channels due to the lower time constant τ_m. The inflow of positively charged sodium ions leads to a positive feedback loop and further depolarizes the cell as more sodium channels are opened. The rapid opening of the sodium activation gates (m gates) is displayed in figure 9 and the high sodium currents are shown in figure 11.

As the membrane potential increases further the slow potassium gates n open, the potassium outflow increases, and the sodium channels are deactivated as the sodium inactivation gate h tends towards 0 in figure 9). When the net outflow of potassium ions exceeds the inflow of sodium ions the membrane potential starts to repolarize back to the resting potential. Since the potassium channels are slow to close more potassium ions flow out of the cell and the potential undershoots, which is known as hyperpolarization. The cell's membrane potential is restored to the resting potential when the sodium inactivation gate h returns to its steady-state value. If the membrane potential reaches the threshold voltage again another action potential can be elicited.

Amplitude Decrease of Action Potentials at 28 °C

This effect can be explained by investigating the gating variables displayed in figure 15. The reason for the amplitude decrease of the action potentials at 28 °C is that the relative refractory period is not yet overcome before a new action potential starts to form. The slow potassium channels n cannot return to their steady-state value of approximately 0.32 before the cell depolarizes again. The reduced membrane potential during hyperpolarization leads to an increase in the necessary current to lift the potential above the firing threshold again to elicit another action potential. However, since the stimulation current is constant at 32 μA in the investigated time frame the amplitude of the resulting action potential decreases.

Interpretation of Phase Plots

Phase plots are an invaluable tool when evaluating dynamical systems as they represent the directional behavior of a system of differential equations. Phase plots can be used to analyze the stability of a dynamic system.

The phase plots in figures 13 and 14 display the relationship between the transmembrane potential and the ion and leakage currents. The state of the dynamical system is described by a tuple of voltage and current. The evolution rule describes what future states can follow from the current state. The trajectories in the plots visualize these voltage/current tuples that occurred in the time frame of the simulation.

As the membrane potential rises/falls the leakage current increases/decreases on a linear trajectory for both temperatures. This is also evident from equation 16 as the current i_L linearly depends on V. The behavior of the sodium and potassium trajectories is more complex. Since the amplitudes of the sodium and potassium currents at 6.3°C are almost identical for each action potential the trajectories lie very close together in figure 13. For 28°C the amplitudes of the sodium and potassium currents are not identical (see figure 12) and hence the trajectories lie further apart in figure 14. The sharper edges of the sodium current/voltage trajectory at 6.3°C are due to the faster opening and closing of the sodium gates. As sodium currents are negative the sodium trajectories lie in the bottom half of the plot in both cases (vice versa for the potassium trajectories).

Comparison LIF and HH Model

The simple leaky integrate and fire (LIF) neuron does not model the ion pump and sets the resting potential by a battery in its equivalence circuit. The LIF model cannot actively produce action potentials and hence a stimulation current has to be introduced. The benefits of the LIF model are that it is computationally lightweight and suffices to model simple questions regarding neuronal behavior.

In comparison, the Hodkin-Huxley (HH) model is a more sophisticated model that is more biophysically meaningful. It models the ion pump and can produce action potentials. Therefore it is suitable to model more complex neuronal behavior. However, this comes at a higher computational cost.

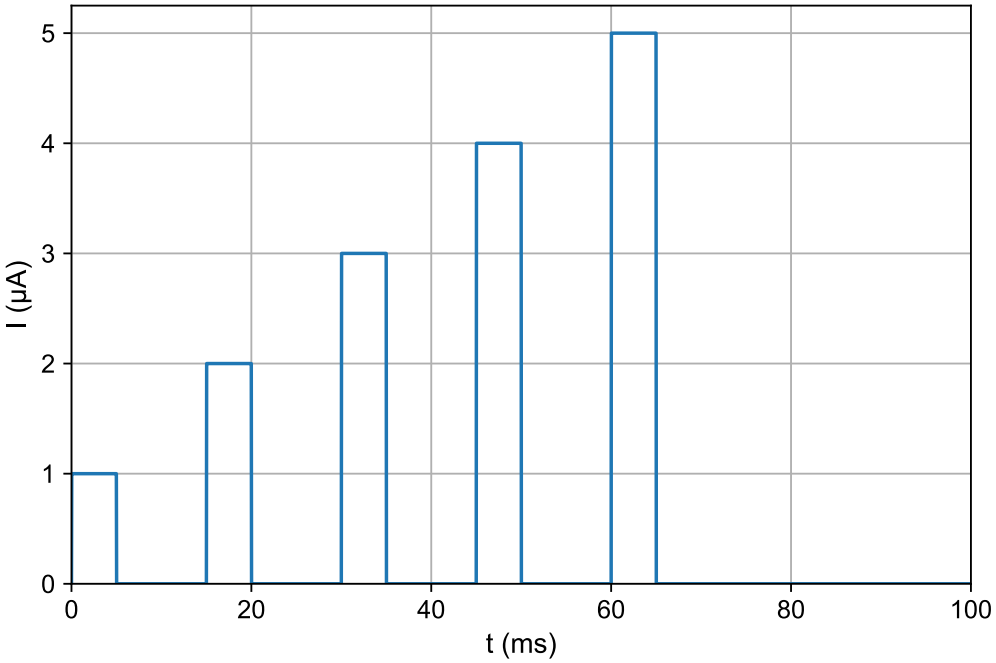

Figure 5: Stimulation current for temperature 6.3 °C

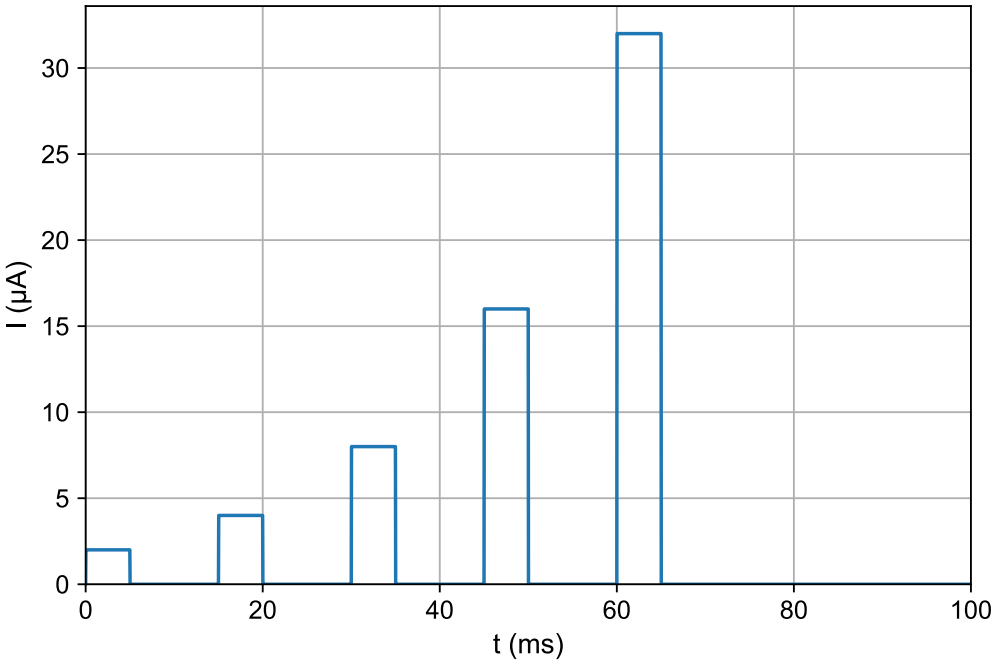

Figure 6: Stimulation current for temperature 28 °C

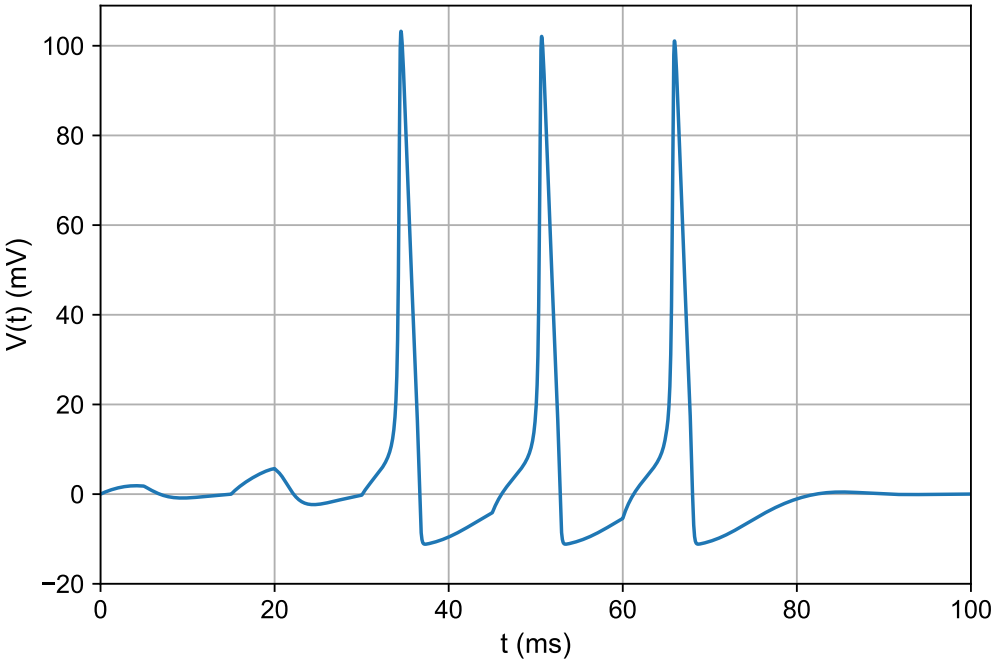

Figure 7: Membrane potential for temperature 6.3 °C

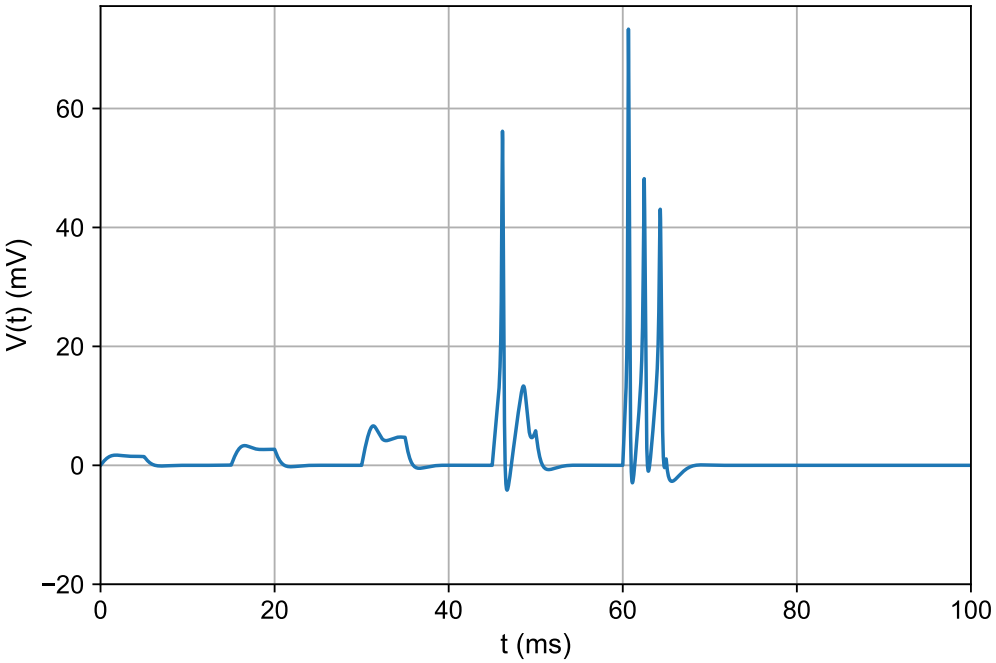

Figure 8: Membrane potential for temperature 28 °C

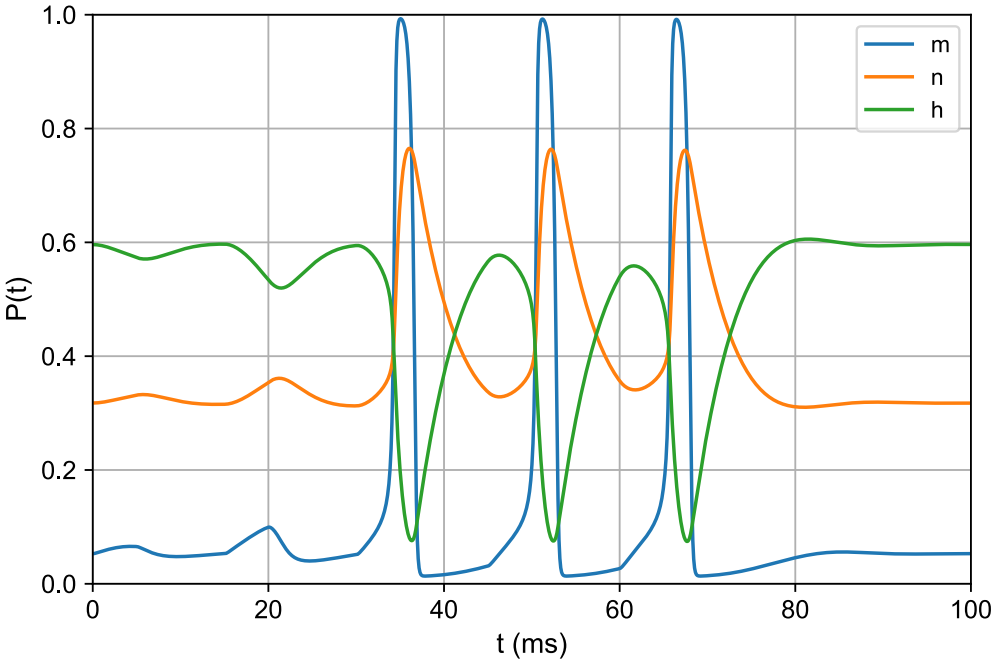

Figure 9: Gating variables for temperature 6.3 °C

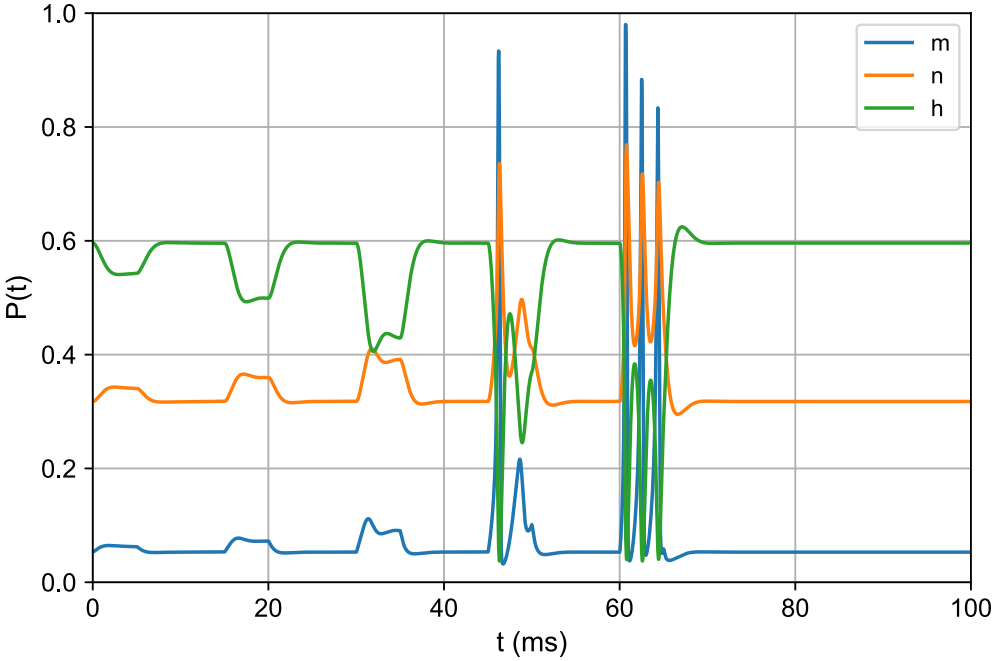

Figure 10: Gating variables for temperature 28 °C

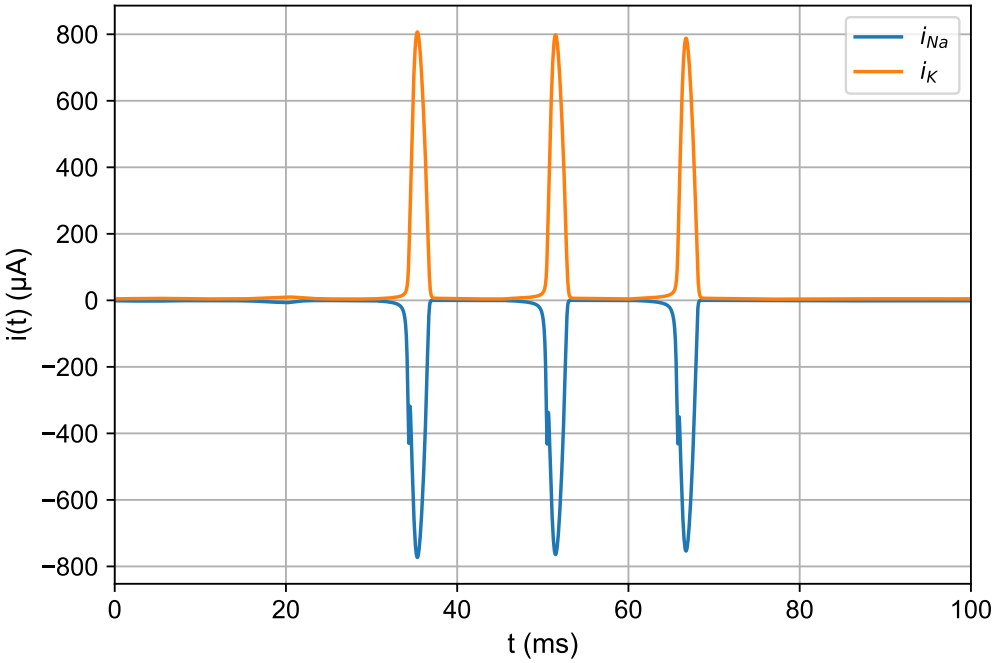

Figure 11: Current densities for temperature 6.3 °C

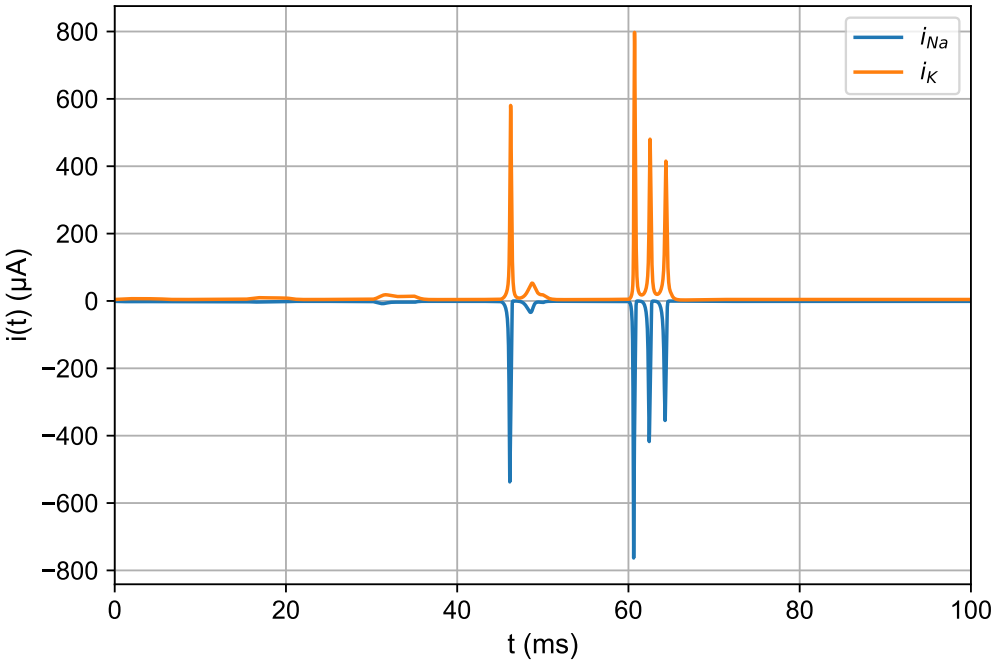

Figure 12: Current densities for temperature 28 °C

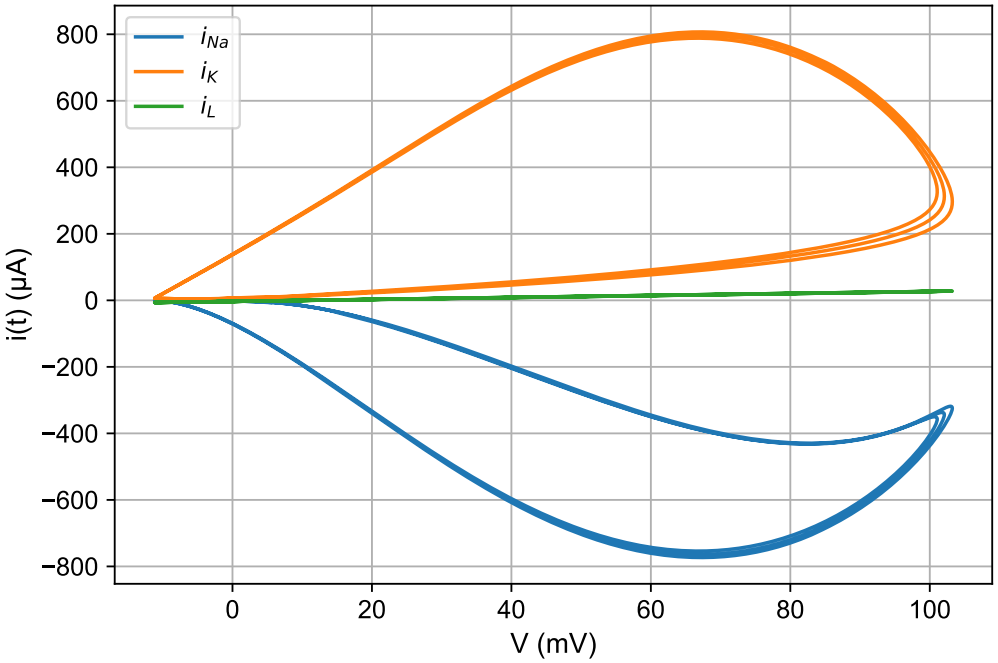

Figure 13: Phase plot for temperature 6.3 °C

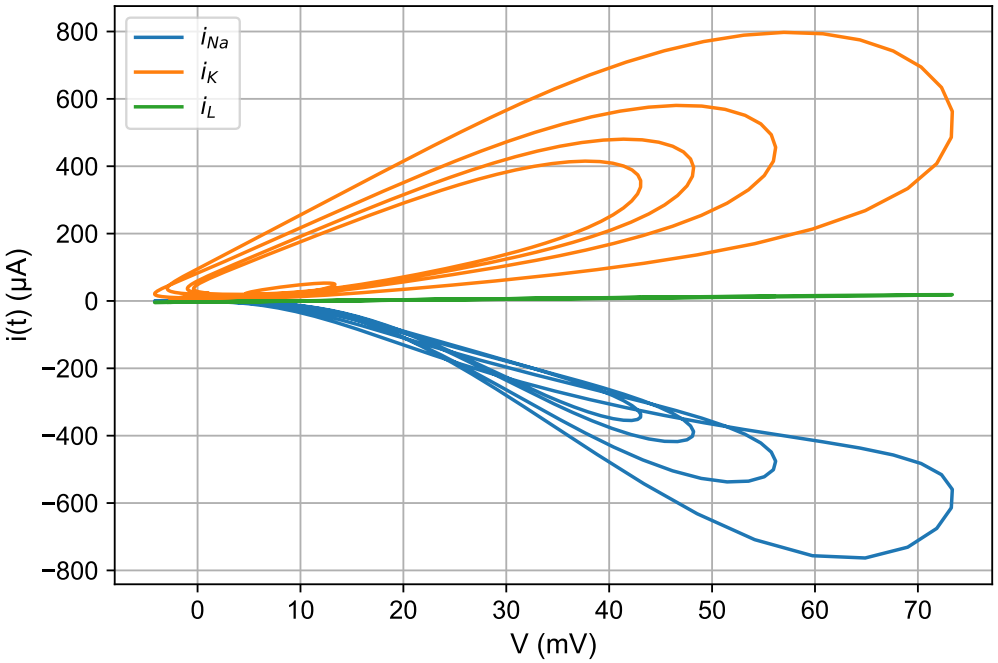

Figure 14: Phase plot for temperature 28 °C

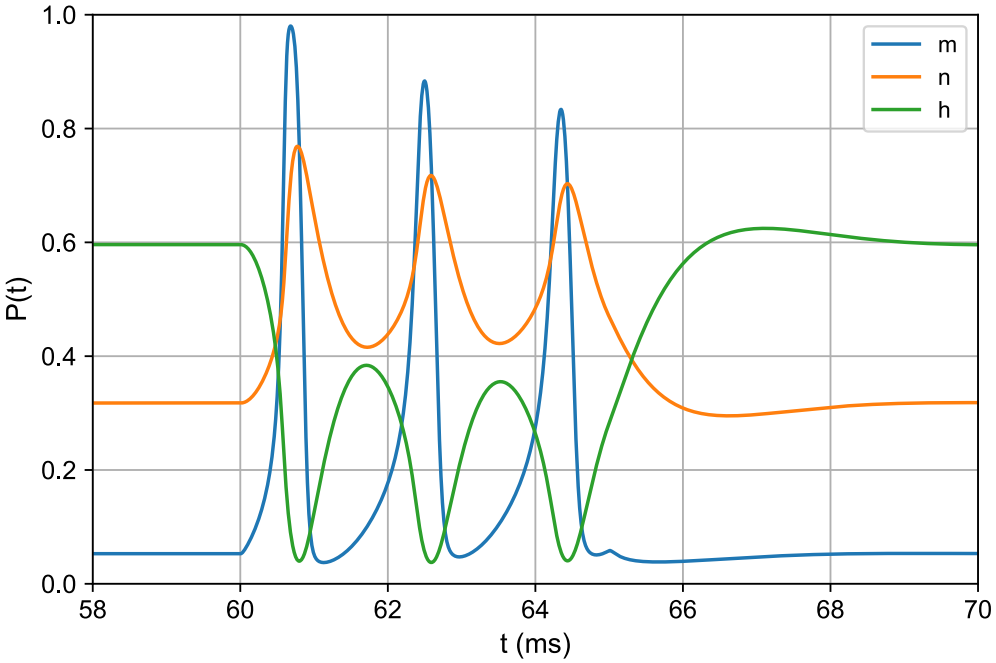

Figure 15: Close-up on gating variables for temperature 28 °C

Neuroprosthetics - Exercise 5

Alexander Koenig

21. December 2019

1 Create a Multi-Compartment Model

The code from the previous programming exercise was altered to model the behavior of a sequence of cells and not just an individual cell. The cable equation and the resulting system of differential equations are solved numerically with the implicit Euler scheme. This results in the following linear system. To calculate the membrane potential in each cell for the next time step the system must be solved for $\vec{x}$.

$$\underbrace{\left(\mathbf{I} - \frac{\Delta t}{C_m R_a}\mathbf{C}\right)}_{\mathbf{A}} \cdot \underbrace{\vec{V}_m(t+\Delta t)}_{\vec{x}} = \underbrace{\vec{V}_m(t) + \frac{\Delta t}{C_m}\left(-\vec{I}_{HH}(t+\Delta t) + \vec{I}_{stim}(t+\Delta t)\right)}_{\vec{b}} \tag{1}$$

$$\mathbf{A} \cdot \vec{x} = \vec{b} \tag{2}$$

100 ms long simulations are run at a temperature of 6.3°C and with a time step of 25 μs. The stimulation currents are rectangular 5ms long pulses with an amplitude of 10 μA. Figures 1 and 2 show the formation and propagation of an action potential along the axon for two different cases. In the first case (figure 1) a pulse stimulates the first compartment only, whereas in the second case the axon is stimulated simultaneously at compartment 20 and 80.

It is evident from both plots that the action potential propagates linearly. This is because the underlying model is a linear system of equations. In figure 2 both action potentials approach each other and destructively interfere at approximately 55 ms. Therefore in figure 2 no signal propagates further than approximately 60ms. This is because the neighboring compartments of the compartment in which the action potentials meet are still in their absolute refractory period.

The three phases (depolarization, repolarization, hyperpolarization) of the action potential can be seen in the plots. The blue area describes the membrane at resting potential ($V_{rest} = 0$). Once the cell depolarizes the membrane potential spikes (red color). Immediately afterward the cell repolarizes (green color) and enters the longer hyperpolarization phase, which can be seen as a darker fade of blue after the action potential.

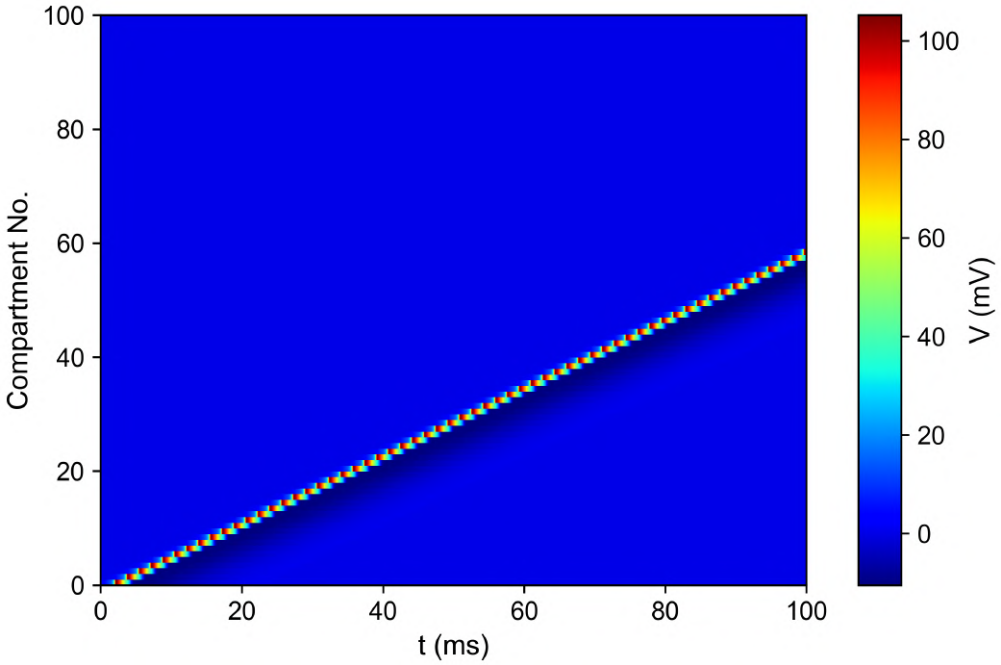

Figure 1: Potential for first case

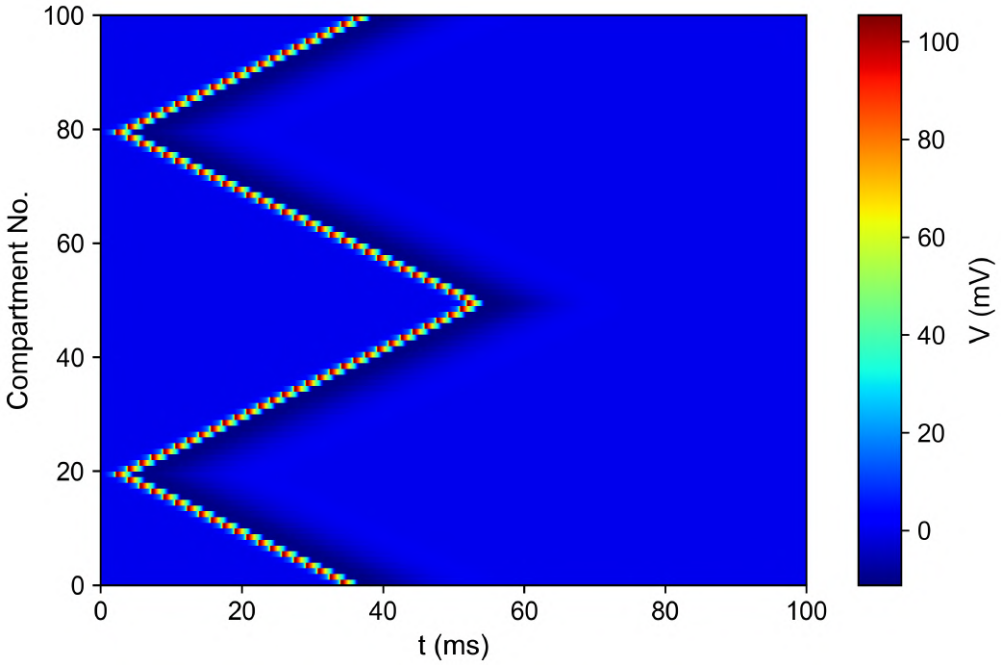

Figure 2: Potential for second case

2 Experiments

The parameters of the model that can be investigated are the membrane capacitance C_m and the axonal resistance R_a. To explore the effect of these variables only the first case from above is investigated since the underlying propagation mechanism is the same in both cases.

Figures 3 and 4 show the effect of increasing and decreasing the parameters with respect to the base case ($C_m = 1\mu F$, $R_a = 7.96k\Omega$). The parameters from the base case are multiplied with the scalars $s \in \{0.5, 1, 1.3, 2\}$ to produce the four plots in each figure. The parameters all control the propagation speed of the action potential. A greater slope in the plot means a higher propagation speed as more compartments are surpassed in less time.

Effects of Axonal Resistance

The axonal resistance depends on three parameters as shown in equation 3. It is directly proportional to the electrical resistivity ρ and the length l of the myelinated axon. The resistance is inversely proportional to the cross-sectional area A of the axon.

$$R_a = \rho \frac{\ell}{A} \tag{3}$$

Figure 3 shows that decreasing the axonal resistance R_a leads to a higher propagation speed. This can be explained with Ohm's law in equation 4. If the resistance decreases at a constant potential the current through the axon must increase. Hence with a higher conductance more current (i.e charges per second) can pass through the axon. Therefore the potential in the adjacent compartment can rise above the firing threshold sooner and the action potential can travel faster. Vice versa increasing the axonal resistance leads to slower signal propagation.

$$R = \frac{V}{I} \tag{4}$$

If the axonal resistance rises above a certain threshold the action potential cannot propagate any further. This is shown in the fourth plot in figure 3. Not enough charge can flow through the axon at once to lift the membrane potential in the adjacent cell above the firing threshold to elicit another action potential.

Effects of Capacitance

Figure 4 demonstrates that the membrane capacitance has a similar effect on the propagation speed as the axonal resistance: reducing the membrane capacitance increases propagation speed and vice versa. Capacitance is reduced by increasing the effective thickness of the membrane, which results in a bigger separation of ions between intracellular and extracellular fluid. Through smaller capacitance, less charged particles are

stored on both sides of the membrane. Thus it is easier to change the membrane potential which allows sodium ions to move more freely along the axon. This results in faster conduction.

Again, it can be observed that if the membrane capacitance rises above a certain threshold the action potential can not propagate further than a few compartments. This is because the membrane capacitance is so high that the stimulating potential from the previous cell is not high enough to induce an ion flow across the membrane, which is needed to form another action potential.

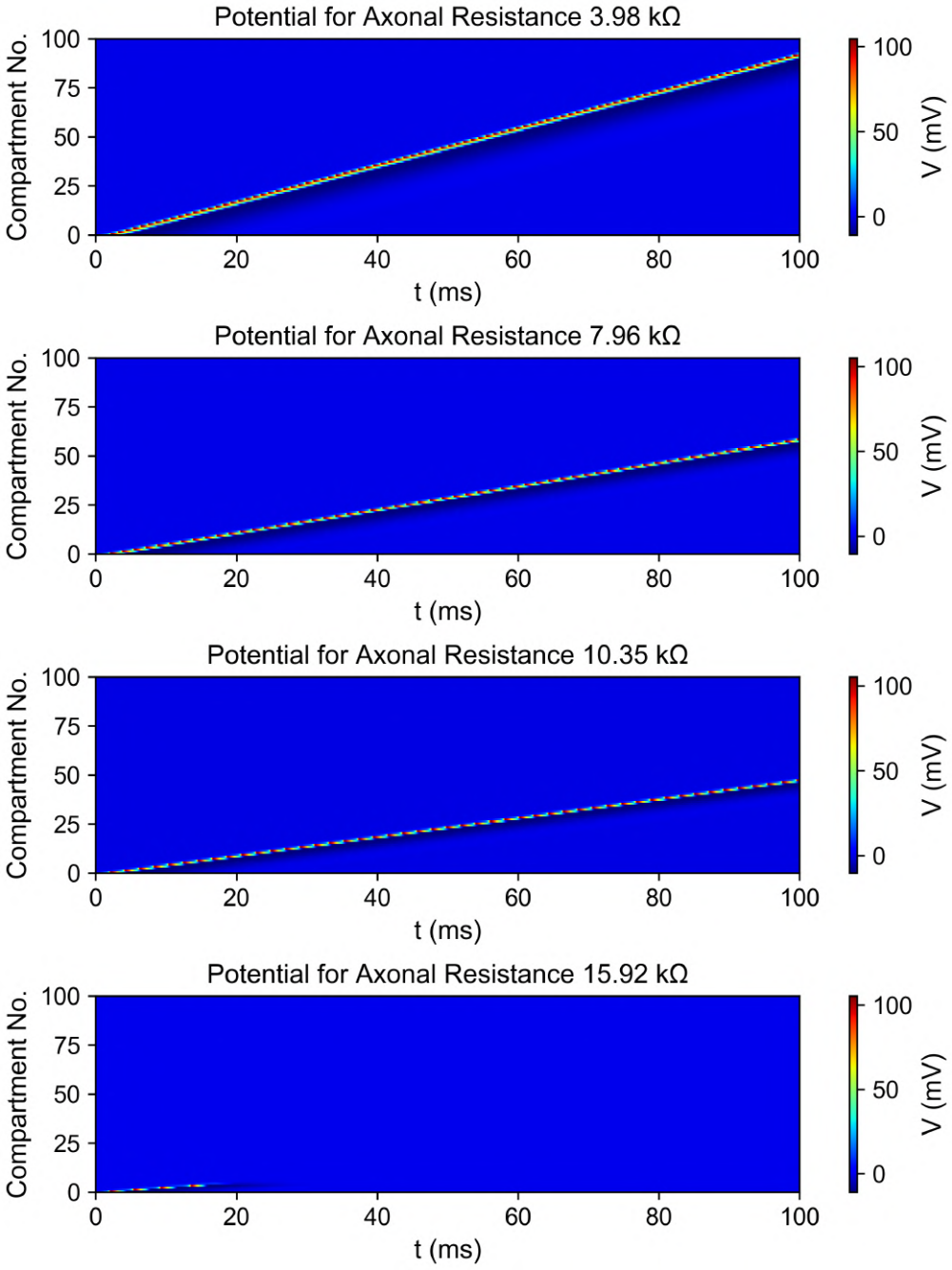

Figure 3: Potential for different resistances

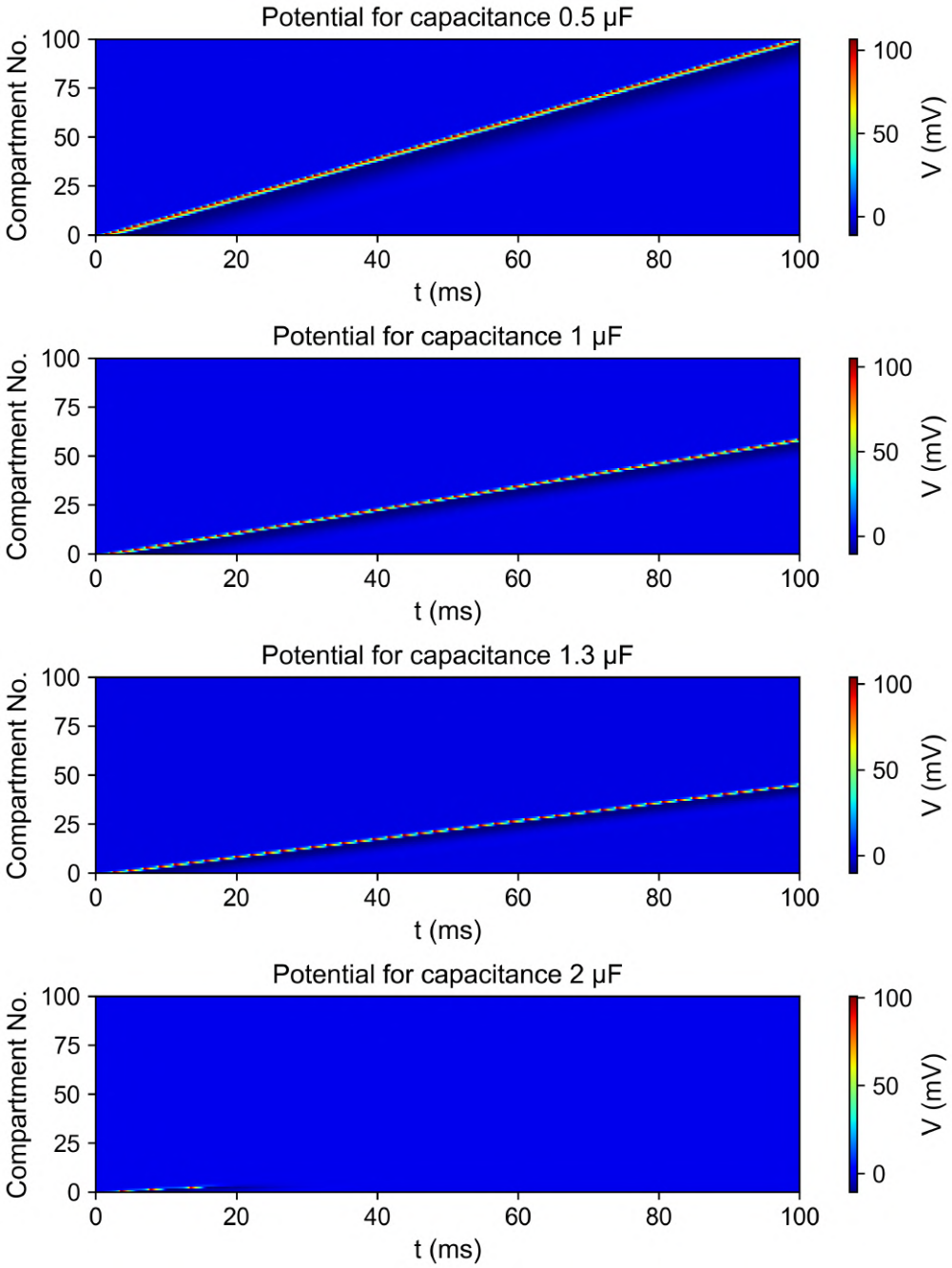

Figure 4: Potential for different capacities

Neuroprosthetics - Exercise 6

Alexander Koenig

21. December 2019

1 Calculate the Potential Field

The potential resulting from a current point source is calculated with equation 1. The potential is directly proportional to the current. A visualization of the potential field for a $50\mu m$ by $50\mu m$ slice at a distance of $10\mu m$ is displayed in figure 1. The current is $I = 1mA$ and the electrical conductivity of the medium is $\rho = 300\Omega cm$.

$$\Phi = \frac{\rho}{4\pi} \cdot \frac{I}{r} \tag{1}$$

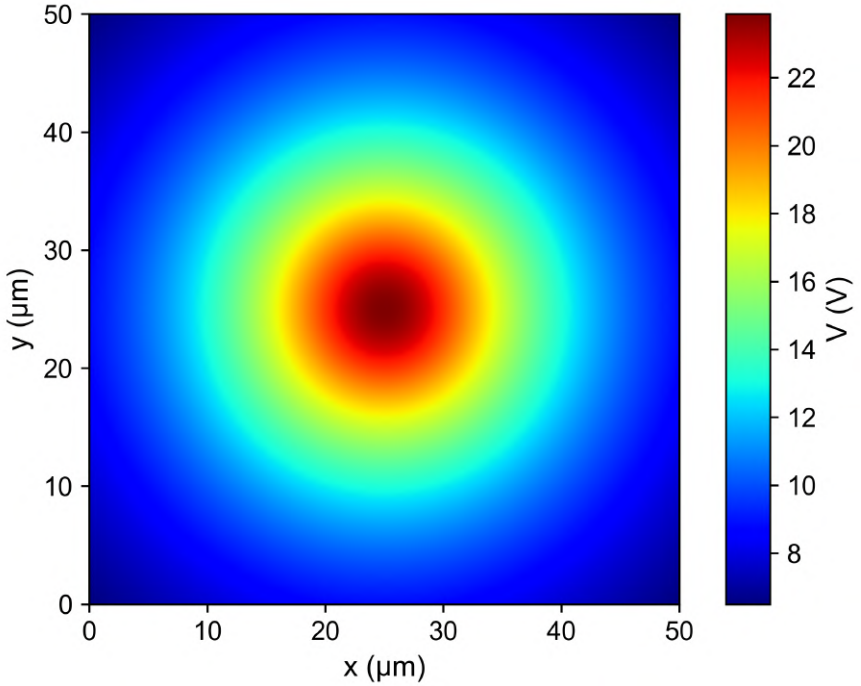

Figure 1: Potential from current source

Figure 2 shows the potential field, the electric field and the activation function in a $50\mu m$ piece of axon positioned $10\mu m$ from the current point source. The three graphs are plotted for an electrode current of $1mA$ and $-1mA$.

From the first two graphs, it becomes clear that the external potential at the axon is positive if the current source is positive (direct proportionality). The potential follows a non-linear profile and reaches its maximum/minimum at the point where the current source is closest to the axon, at $25\mu m$.

The electric field is defined as the negative first spatial derivative of the potential (in absence of a magnetic potential). Hence the electric field follows the displayed trajectory, with two peaks/throughs where the change of the potential is smallest/greatest. The electric field is zero at the point where the potential reaches its maximum/minimum.

The activation function is calculated as the second derivative of the external potential. It is evident from the plot that the activation functions for both currents have their maximum/minimum at the point where the potential reaches its minimum/maximum. The activation function describes the activation of the neuron due to an external potential.

2 Calculate a Neuron Model

The model from exercise 5 is enhanced to model the influence of an external potential on the axon. The axon is positioned as in section 1 and simulations are run with different stimulation sequences. The phase duration of all pulses is 1ms.

- Figure 3 shows that the current pulse is too weak to elicit an action potential. The positive activation only lifts the membrane potential to approximately 1.6mV and does not reach the firing threshold. The compartments around the peak experience a negative activation and hence show a darker shade of blue in the plot. There is a small undershoot of the membrane potential after the current pulse due to the slow closing of the potassium channels.
- Figure 4 shows the clear formation of an action potential. The current pulse of -1mA results in a strong enough neuronal activation to lift the membrane potential above the firing threshold. The signal then propagates linearly in both directions, like in the previous exercise.
- Figure 5 shows a similar situation as in figure 3. The first phase of the bi-phasic current pulse can not lift the membrane potential above the threshold and no action potential can form. The simulation differs from the simulation in figure 3 in that the rise of the membrane potential is much shorter as the second phase of the pulse immediately reduces the membrane potential with its negative activation (positive potential leads to negative activation in the middle compartments of the axon).

- Figure 6 shows that the formation of an action potential is possible using a biphasic current pulse if the first pulse is strong enough.
- Figure 7 shows that a positive current pulse reduces the membrane potential in the middle compartments due to its negative activation. The membrane potential in the outer compartments rises, but at approximately 0.3mV it is far from the firing threshold. No action potentials can be elicited.
- Figure 8 demonstrates that if a positive current pulse is strong enough multiple action potentials can be elicited. Approximately at compartments 20 and 80, the membrane potential is lifted above the firing threshold by the positive parts of the activation function. Two action potentials form from these two points and a third one is elicited in the middle compartments at roughly 15ms. The outer action potentials travel towards the inner one and destructively interfere because the neighboring compartments of the compartment in which the action potentials meet are still in their absolute refractory period.

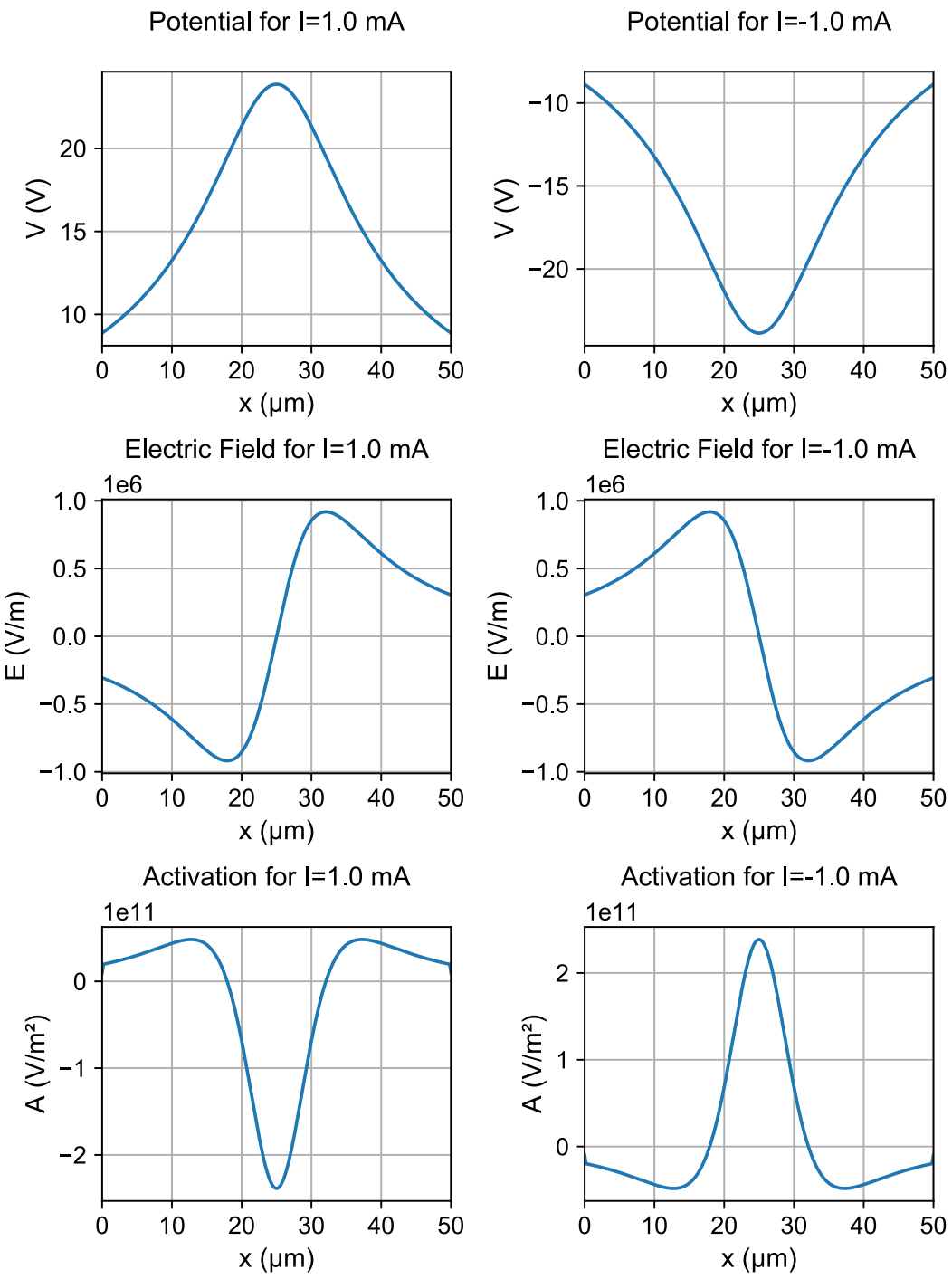

Figure 2: Potential, electric field and activation function for different currents

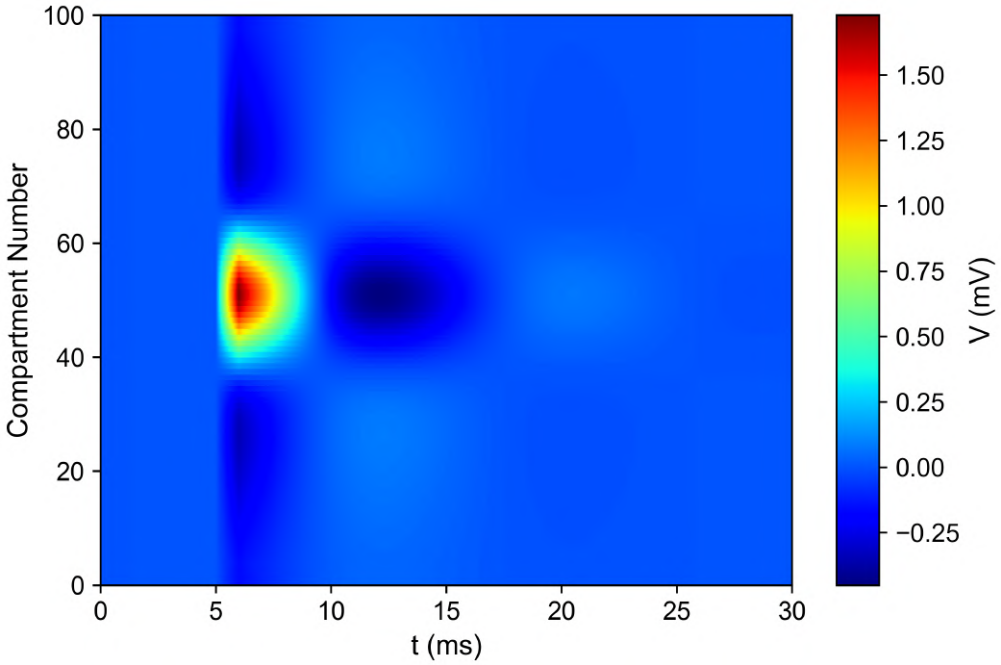

Figure 3: Stimulation type: mono-phasic, Current: -0.25mA

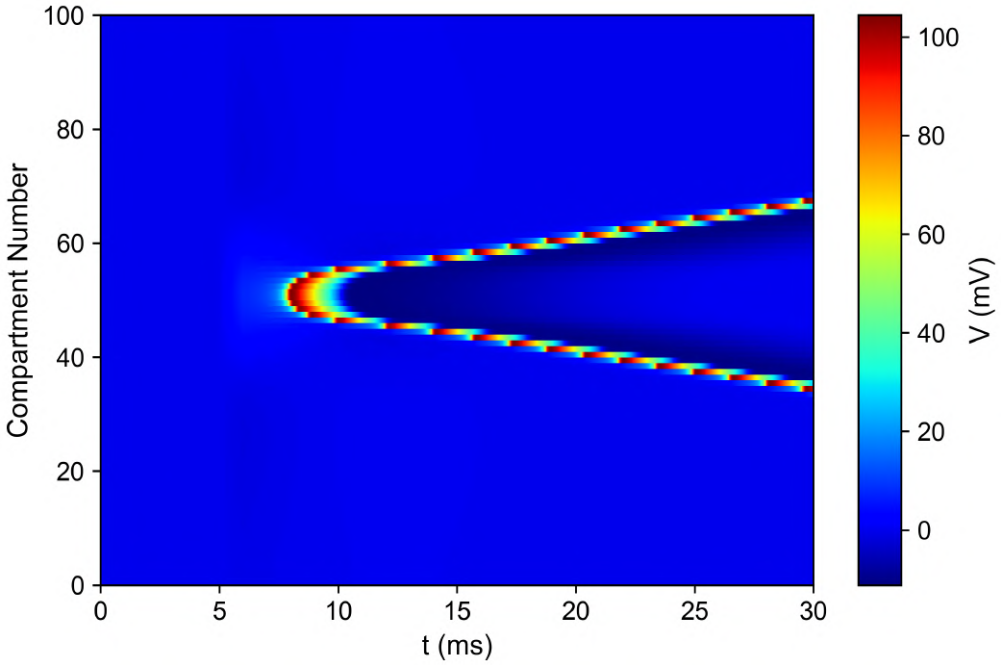

Figure 4: Stimulation type: mono-phasic, Current: -1mA

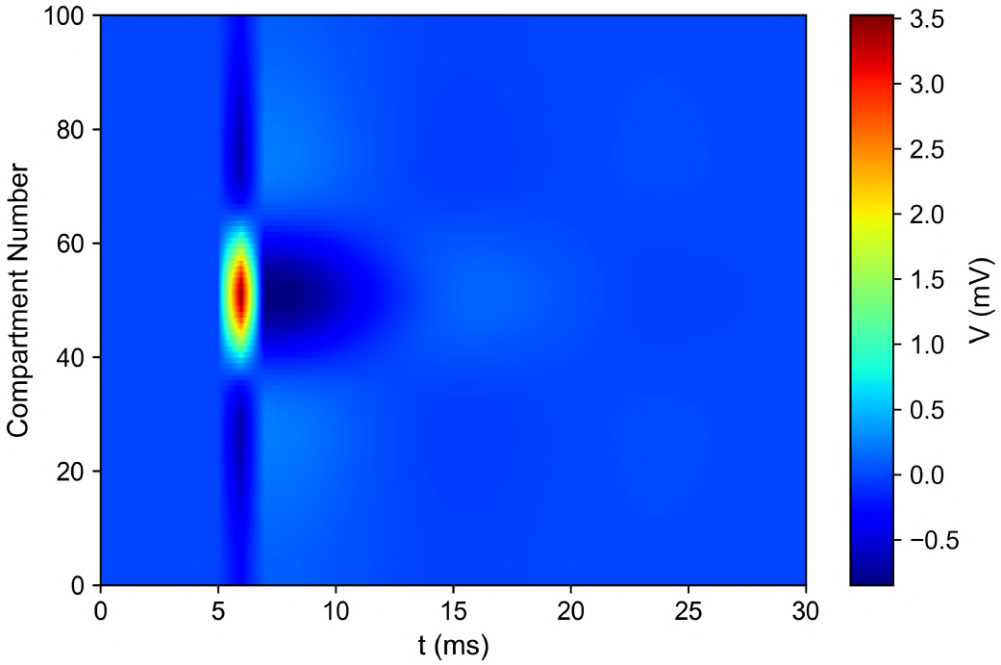

Figure 5: Stimulation type: bi-phasic, Current amplitude: 0.5mA

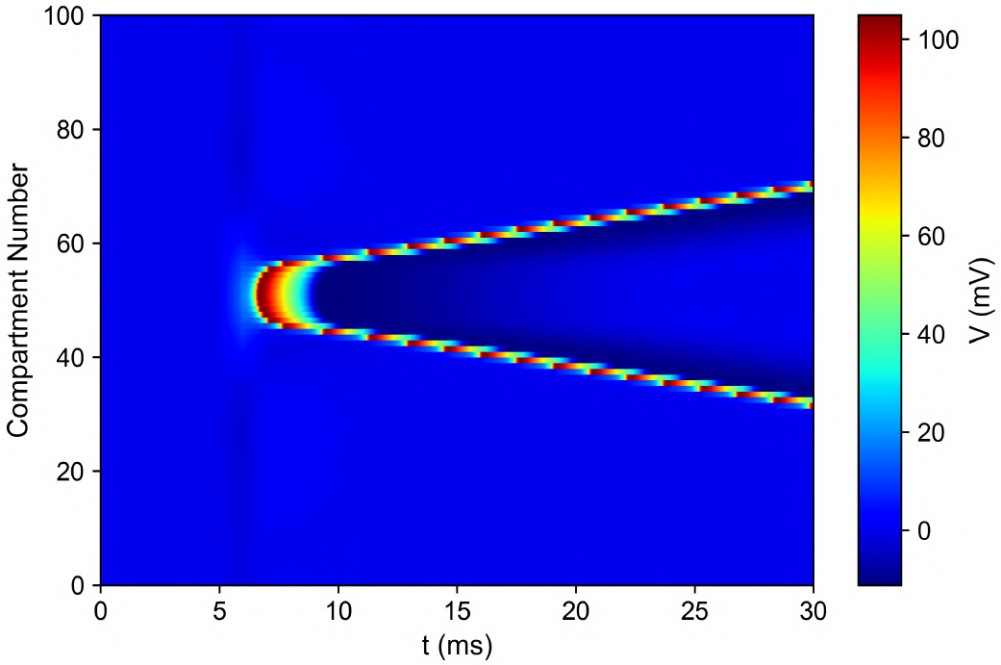

Figure 6: Stimulation type: bi-phasic, Current amplitude: 2mA

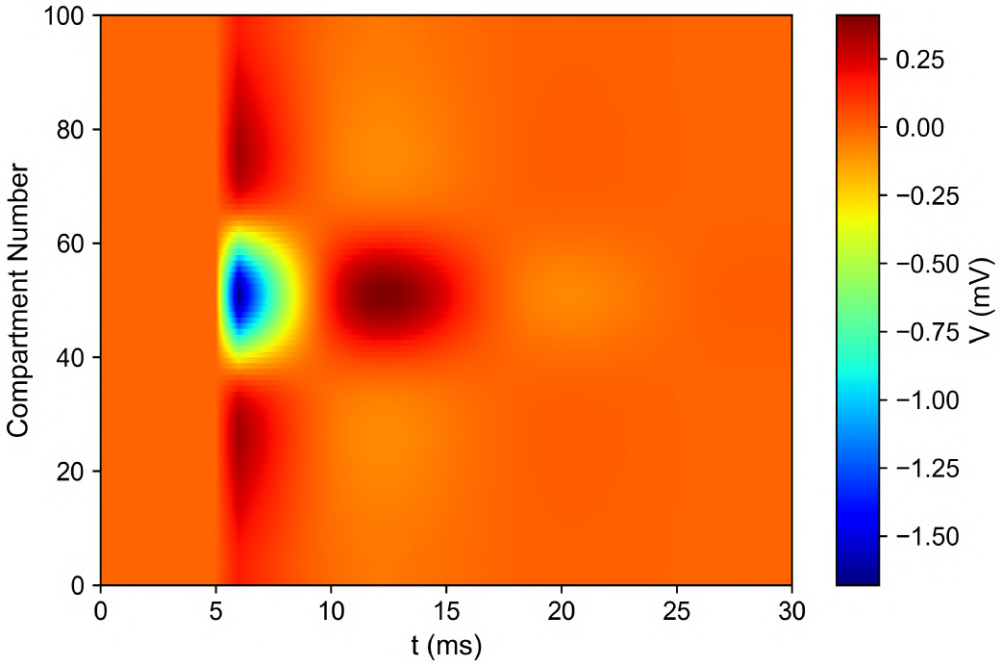

Figure 7: Stimulation type: mono-phasic, Current: 0.25mA

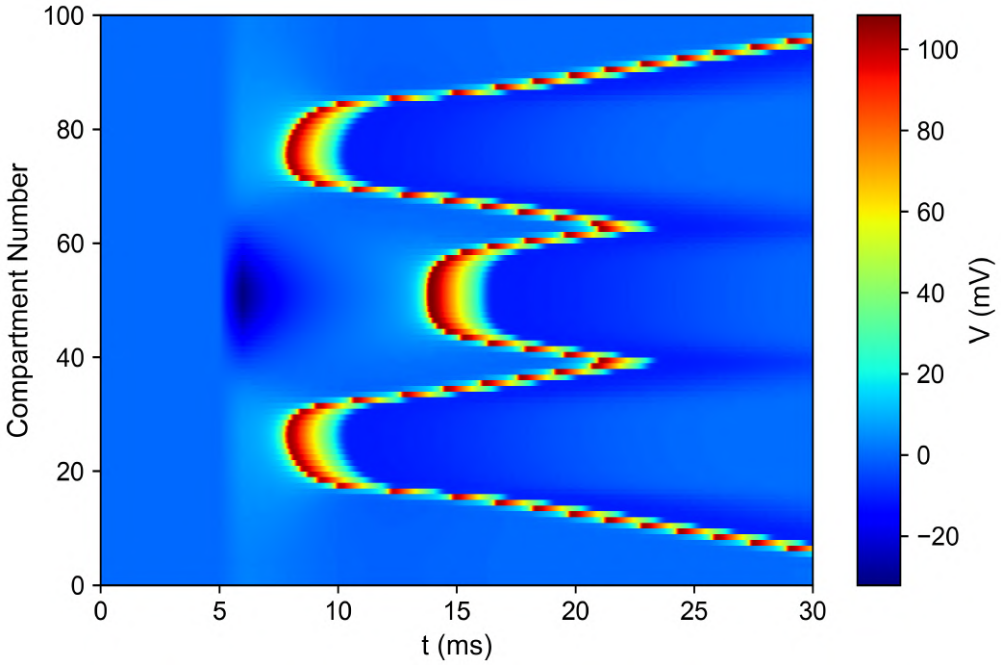

Figure 8: Stimulation type: mono-phasic, Current: 5mA

Neuroprosthetics - Exercise 7

Alexander Koenig

26. January 2019

1 Border Frequencies of a Filter

The simplified Cochlear Implant (CI) consists of $n \in \{3, 6, 12, 22\}$ electrodes and uses a bandpass filter for each electrode on the array. The border frequencies of each electrode are logarithmically distributed between an overall range of 100Hz for the most apical electrode to 8 kHz for the most basal electrode. Below is a list of the border frequencies (in Hz) for each electrode array. Figure 1 shows a logarithmic plot of the border frequencies of a cochlear implant with 22 electrodes.

- $n = 3$: [100. 431. 1857. 8000.]
- $n = 6$: [100. 208. 431. 894. 1857. 3854. 8000.]
- $n = 12$: [100. 144. 208. 299. 431. 621. 894. 1289. 1857. 2675. 3854. 5553. 8000.]
- $n = 22$: [100. 122. 149. 182. 222. 271. 330. 403. 492. 601. 733. 894. 1092. 1332. 1626. 1984. 2421. 2955. 3606. 4401. 5371. 6555. 8000.]

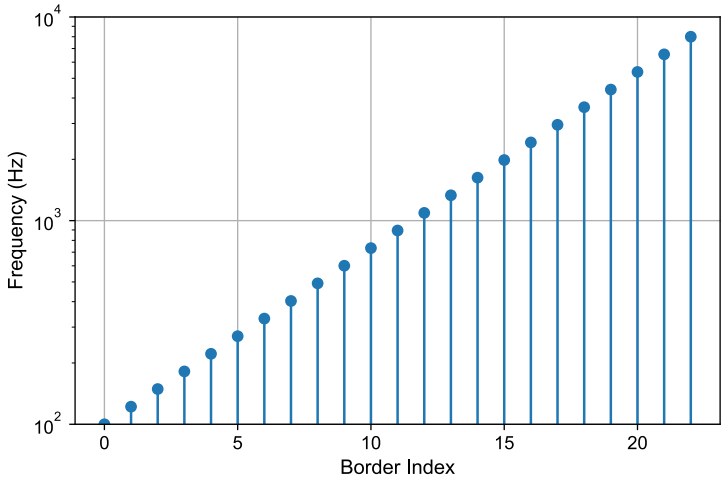

Figure 1: Border frequencies of CI with 22 electrodes

2 Implement a Filter Bank

A second-order bandpass filter bank was implemented for the cochlear implants with the above border frequencies using the Butterworth bandpass filter. Butterworth filters feature a cutoff frequency of -3.01dB at the border frequencies and a maximally flat filter response in the passband. When viewed on a logarithmic plot the response rolls off linearly towards negative infinity at a rate of -12dB per octave for second-order filters. Figure 2 and 3 show the frequency response of the filter bank for 3 and 22 electrodes respectively.

The phrase "Koenig's Test Word" was recorded with a microphone and filtered with the filter banks. The time signal of each filter channel of a 12-electrode CI is plotted in figure 4. The blue lines represent the original sample, whereas the orange plot represents the sound at the electrode. By investigating the plotted results and by listening to each filter channel it becomes evident that some electrodes can represent specific spoken letters. For example, electrodes 1 to 4 mainly catch the lower sound of the "oe" in "Koenig's Test Word". The highly pitched "s" sounds in the words are captured by electrode 12. Here three distinct peaks in the signal at both "s" sounds and at the "t" can be identified.

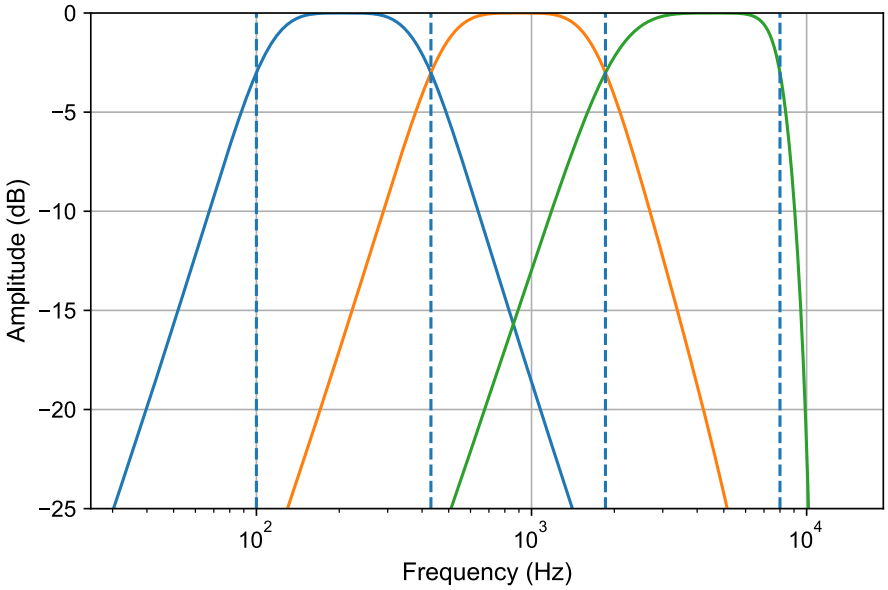

Figure 2: Frequency response for 3-electrode filter bank

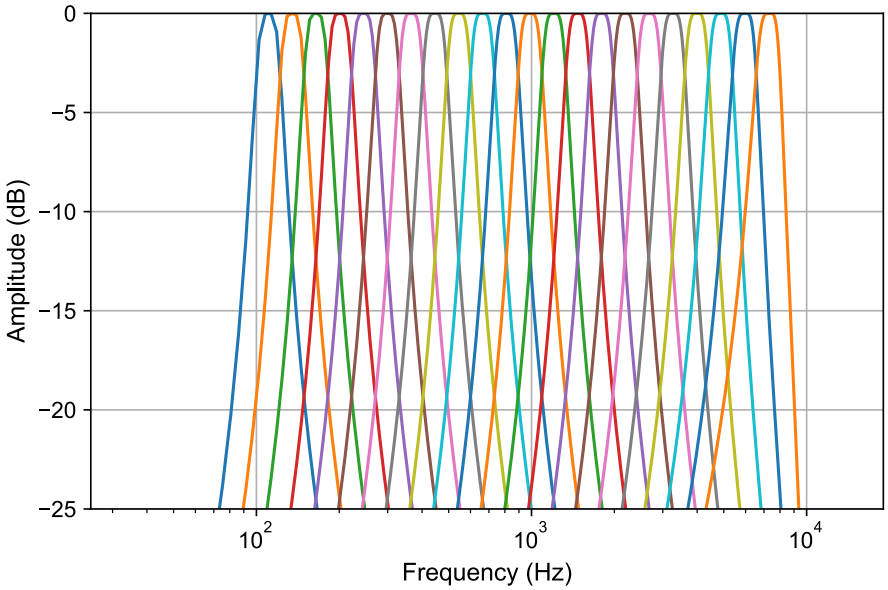

Figure 3: Frequency response for 22-electrode filter bank

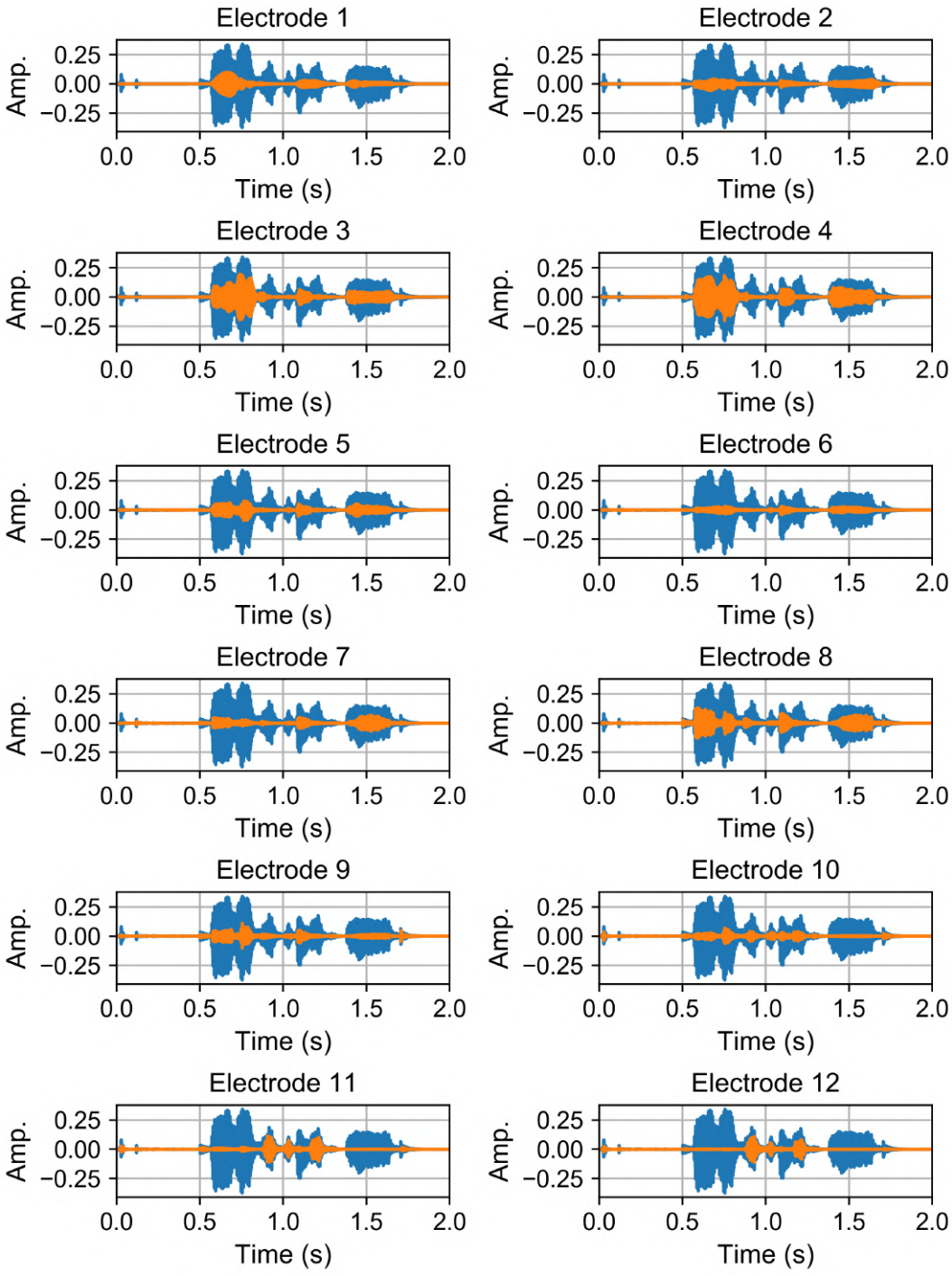

Figure 4: Amplitude at each electrode

3 Join the Channels

In this section, the individual signals at each electrode are summed back together in order to compare them to the original signal. For reference figures 5, 6 and 7 show the amplitude, spectrum and spectrogram of the original signal, respectively. Figures 8, 9 and 10 display the same data for each CI, but this time reconstructed from the electrode array of the cochlear implant. When one listens to the summed output of the electrode array the signal can almost not be distinguished from the original sound, even for the CI with 3 electrodes.

The similarity of the signals can also be seen from the spectrograms - they are almost identical for each CI. The reason for this is that the whole audible spectrum is covered by the filters. In the spectrogram, one can observe each of the three words ("Koenig's", "Test", "Word") as a distinct area.

From figure 9 it becomes clear that the higher the number of electrodes, the more power is lost. This may be due to the fact that there are more border areas which are attenuated by -3dB. This effect can also be observed in the amplitude plots in figure 8 where the amplitude of the signals decreases the more electrodes there are.

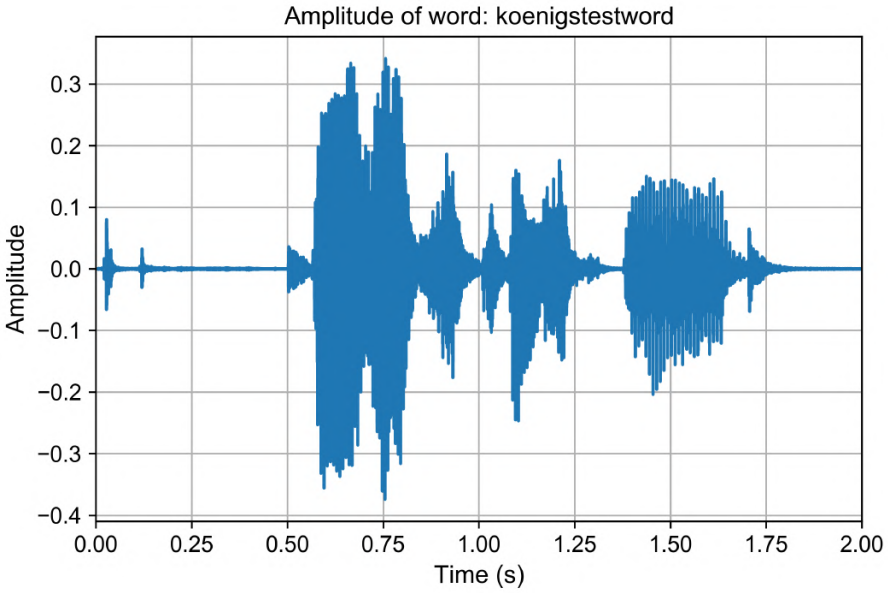

Figure 5: Amplitude of original signal

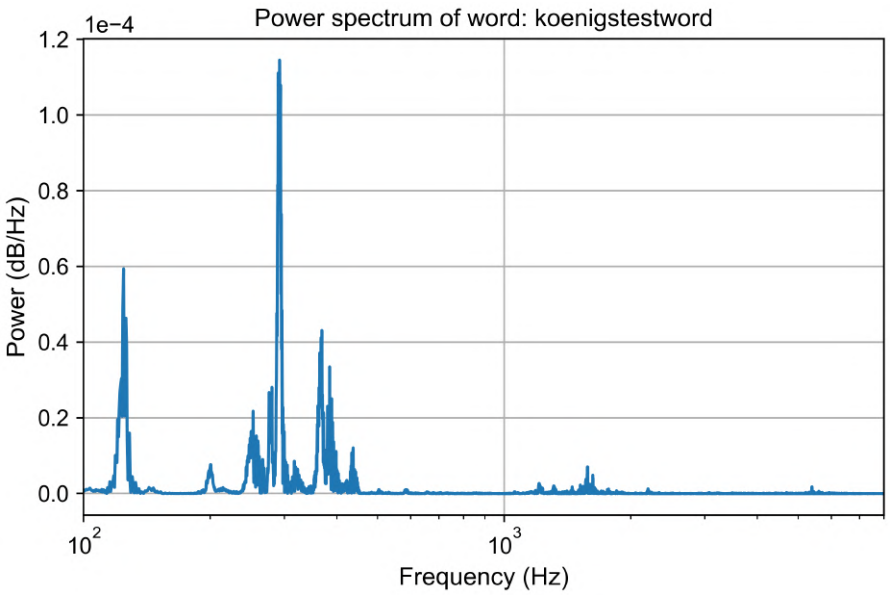

Figure 6: Power spectrum of original signal

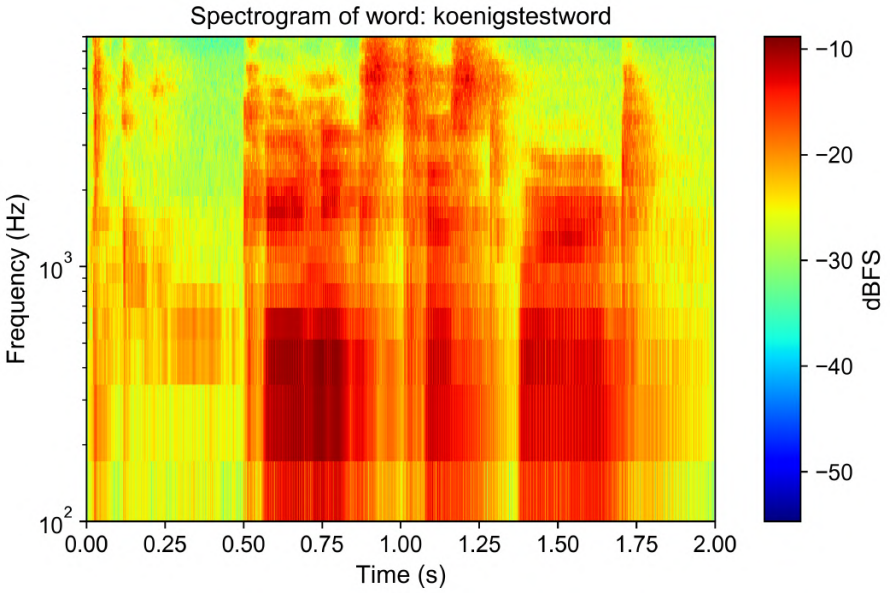

Figure 7: Spectrogram of original signal

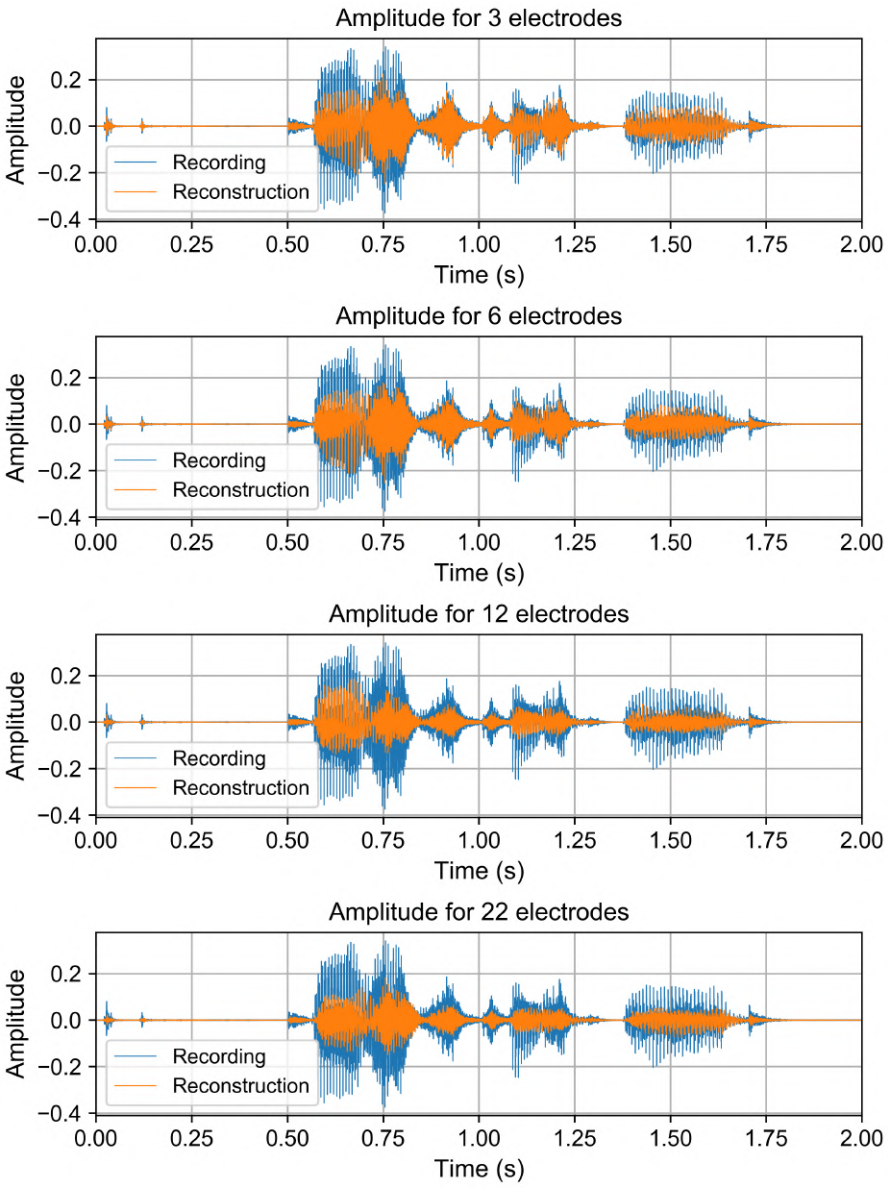

Figure 8: Amplitude of the summed signals for each CI

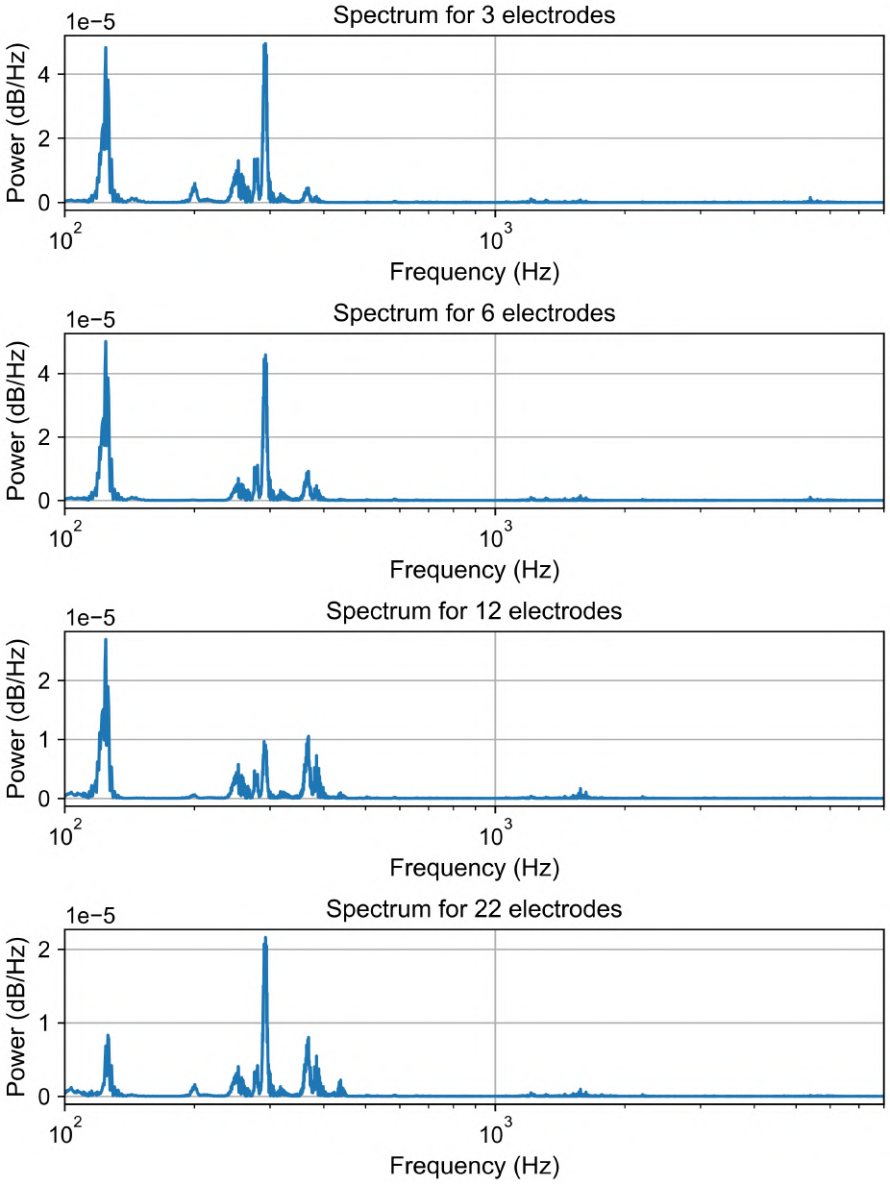

Figure 9: Power spectra of the summed signals for each CI

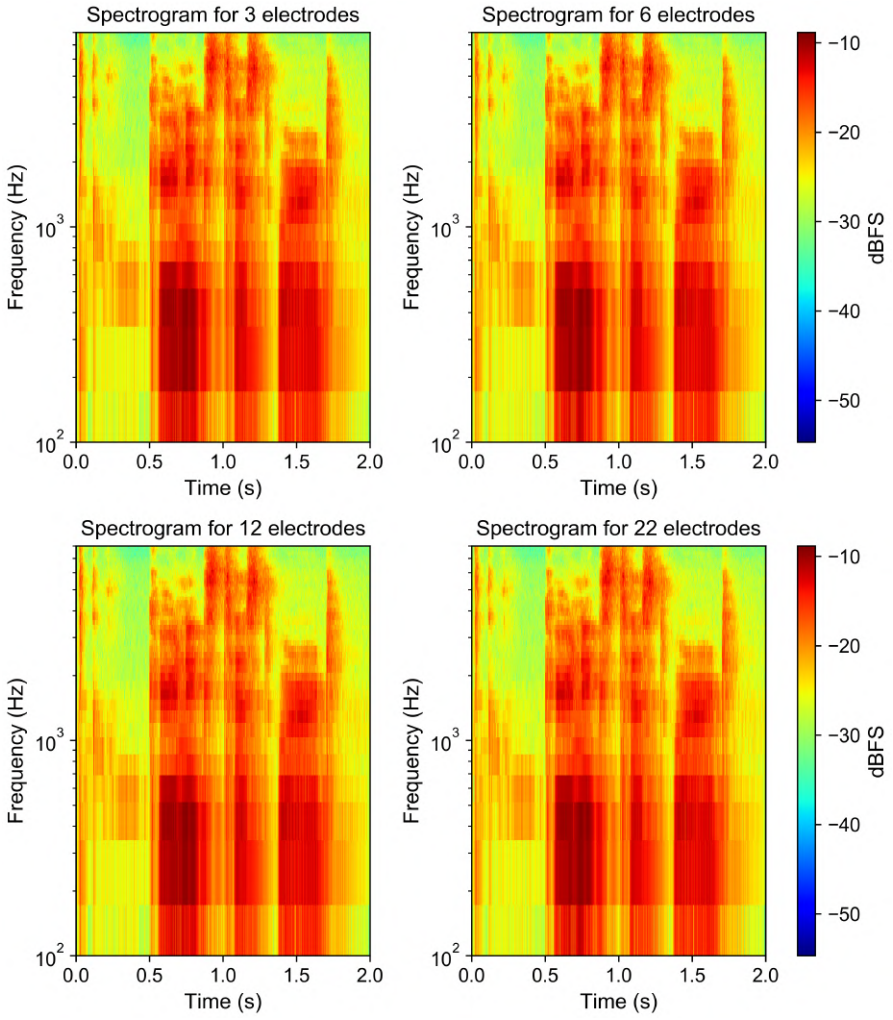

Figure 10: Spectrograms of the summed signals for each CI

Neuroprosthetics - Exercise 8

Alexander Koenig

31. January 2019

1 Noise Vocoder with Dynamic Compression

In this exercise, a noise vocoder with dynamic compression is implemented to model the sound impressions a patient using a cochlear implant (CI) is hearing. In order for this to work white noise with a Gaussian distribution (mean 0, standard deviation 1) is filtered with the filter banks from exercise 7. The filtered noise is then modulated with the envelopes of a filtered speech signal. The envelopes are generated with a Hilbert transform. The envelopes for a CI with 12 electrodes are displayed in figure 1. The same word ("Koenig's Test Word") as in the previous exercise is used in this exercise.

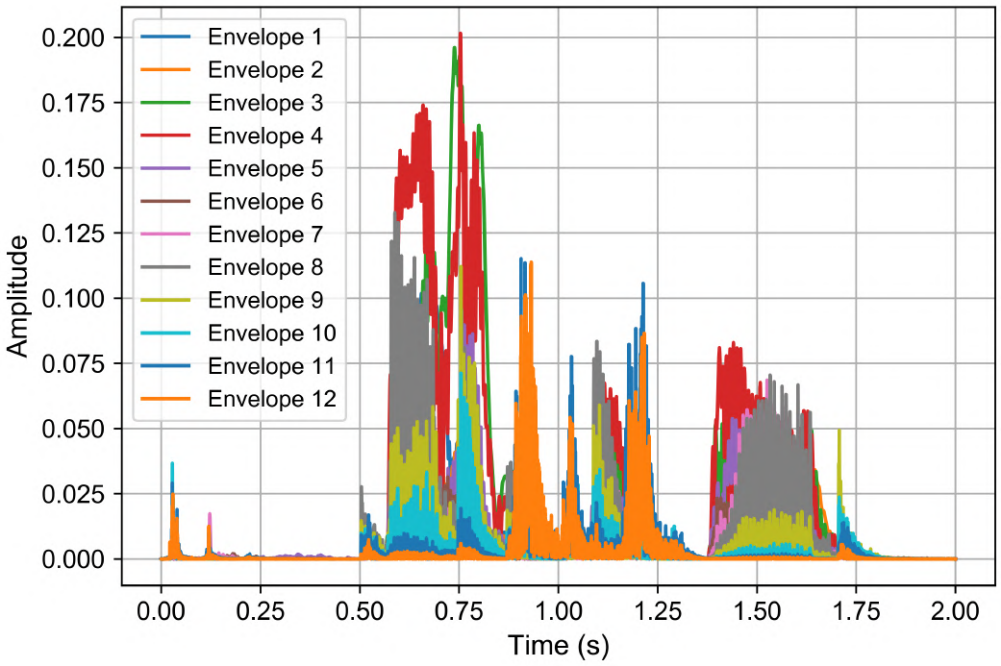

Figure 1: Envelopes for 12 electrode-CI

In the next step dynamic compression according to equation 1 is applied to the envelopes. The variable c is the compression rate, which is set to 500. After the compression, all values above a threshold of 1 are clipped to a value of 1 and all values below a custom threshold are clipped to 0. Figure 2 shows the processed envelopes with a lower threshold of 0.2. It is obvious that the higher threshold of 1 is never reached, but all amplitudes below 0.2 are clipped to 0.

$$\mathrm{env}_{\mathrm{compressed}} = \frac{\log_{10}(1 + c \cdot \mathrm{env})}{\log_{10}(c + 1)} \tag{1}$$

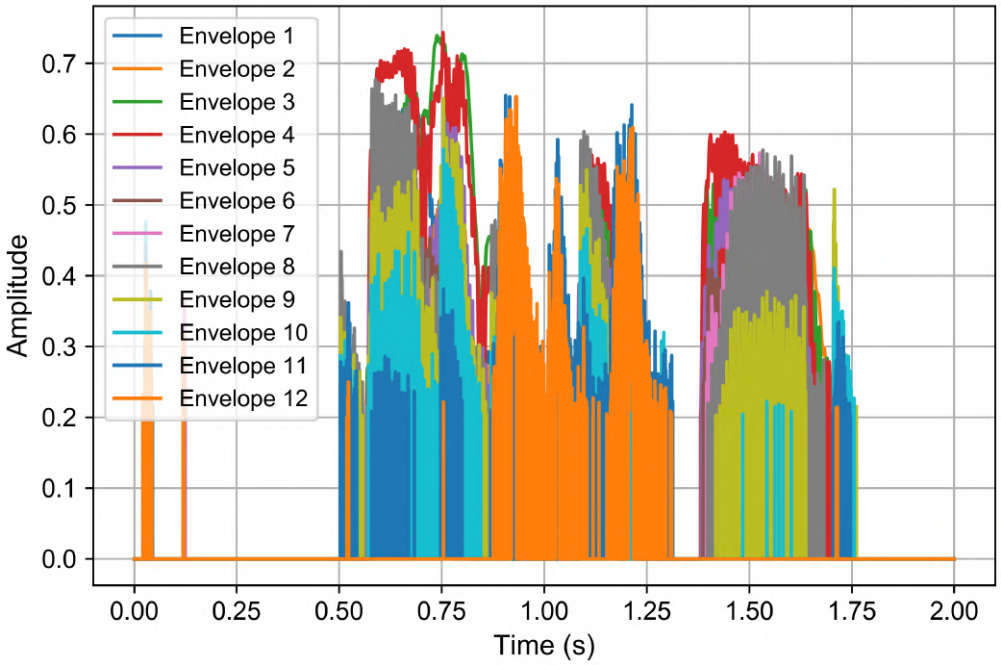

Figure 2: Compressed and filtered envelopes for 12 electrode-CI

In the next step, the processed envelopes are modulated with the noise to model the signal that the patient will hear. After this, the signals at each electrode of the CI are summed back together to get an overall acoustic impression. Figures 3, 4 and 5 show the amplitudes, the spectra and the spectrograms of the original and the reconstructed signal for a 12-electrode CI, respectively.

Figure 3 demonstrates that the reconstruction process with the introduced noise "smudges" out the signal. The peaks are less distinct, making the signal less intelligible. Also, the amplitude of the signal is increased. Figure 4 shows that the induced noise is also visible in the power spectrum. Almost all frequencies have a power greater than zero - which comes from the white noise generated in the beginning. Finally, figure 5 shows that the

words (three dark red areas in the top figure) are less distinct in the noisy reconstruction. Further, some parts of the signal do not appear in the spectrogram at all because the amplitude of the compressed envelope was below the clipping threshold.

When listening to the summed up signals, which represent the signal the patient hears, it becomes clear that the more electrodes the CI has, the better the reconstruction quality becomes. While the signal for 3 electrodes is almost not understandable and purely noise, the word reconstructed by a 22-electrode CI can be understood well. Increasing the threshold from 0.2 to higher values removes more parts of the signal and hence reduces the comprehensibility of the word. At lower compression rates the signal seemed to be better intelligible than for higher ones. Higher-order (e.g. order 8) bandpass filters only produced loud noises and no good reconstruction. Using lower order (e.g. order 2) filters seems to produce lower quality results.

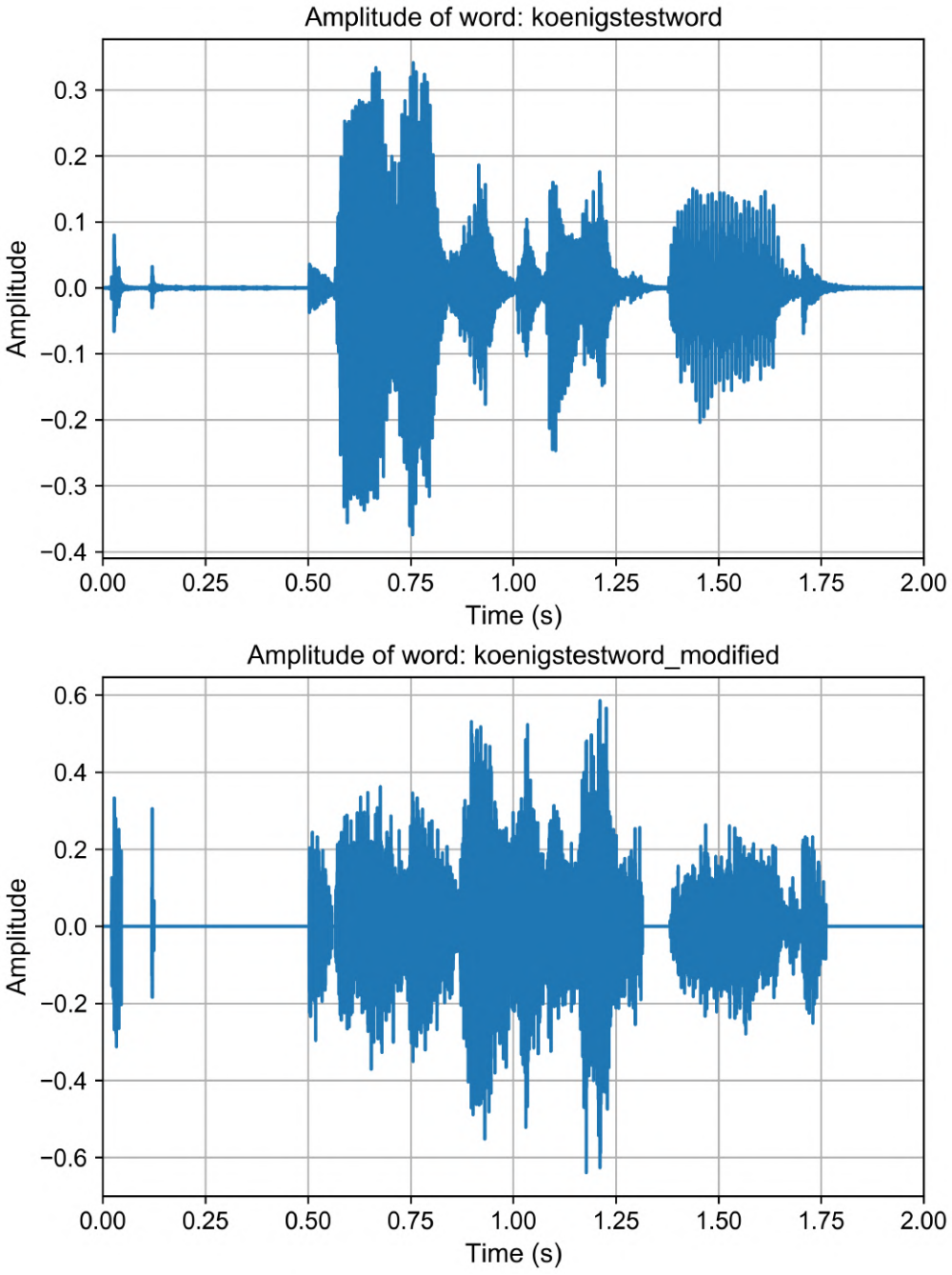

Figure 3: Amplitudes of original and reconstructed signals

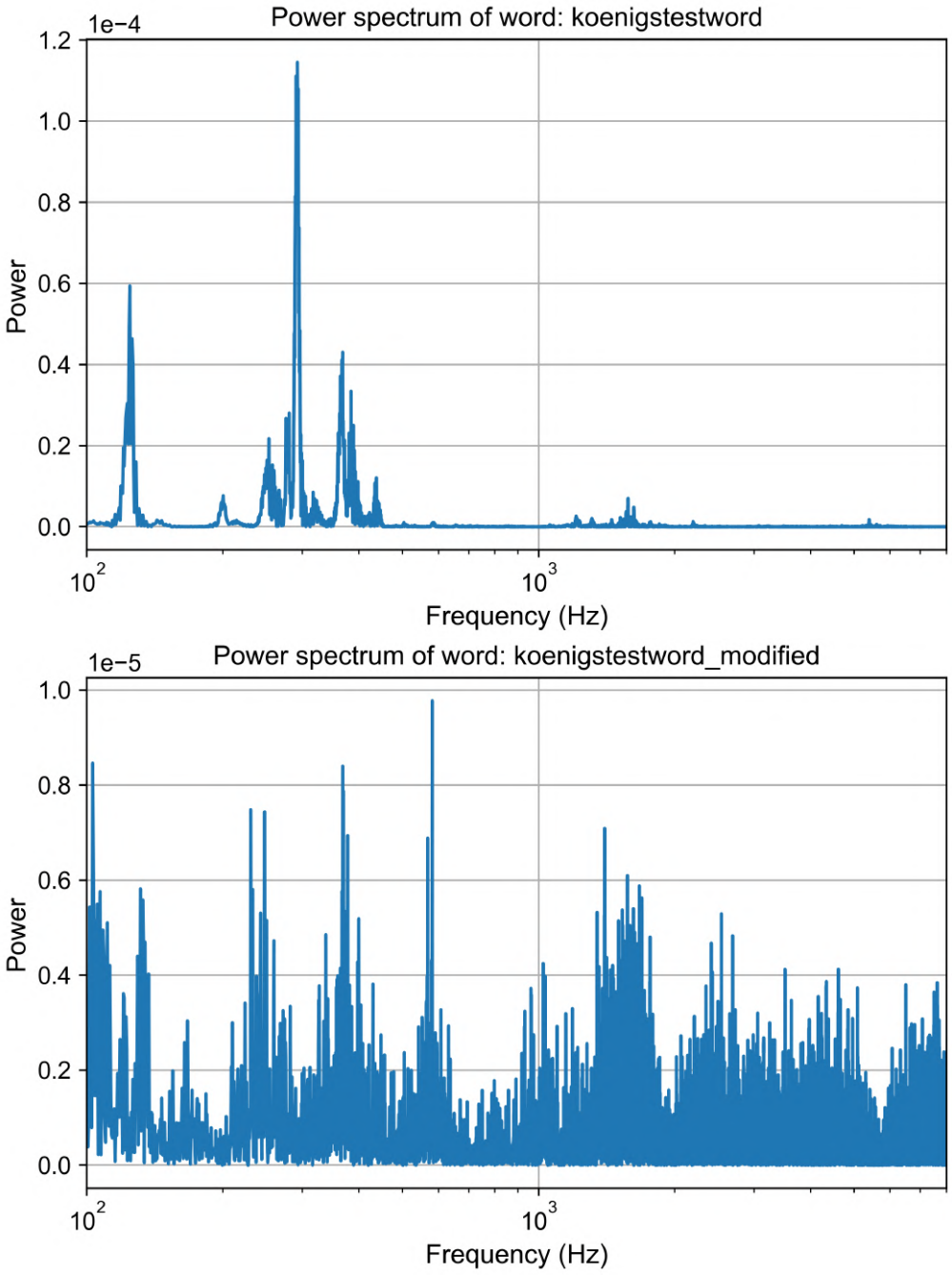

Figure 4: Spectra of original and reconstructed signals

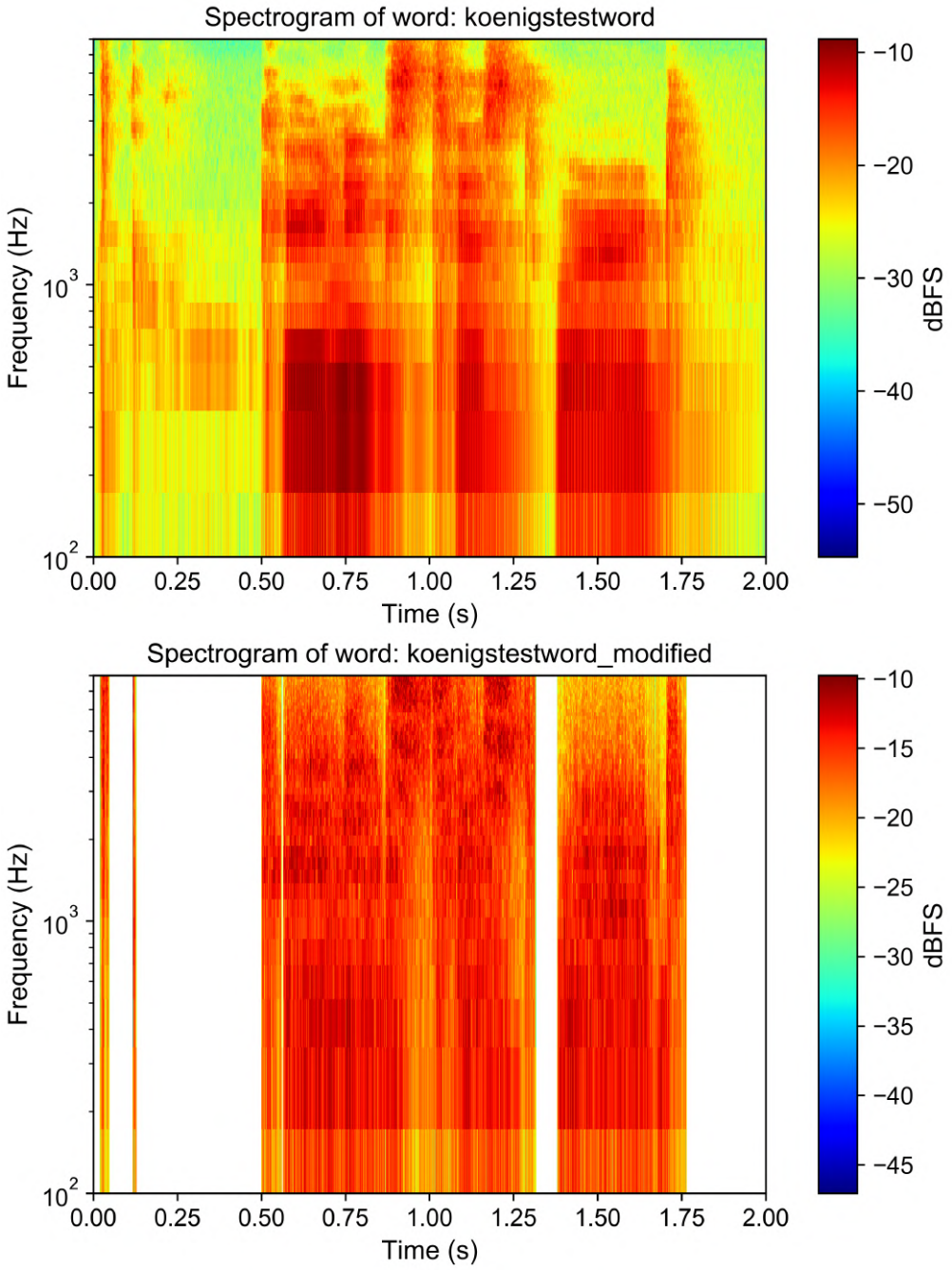

Figure 5: Spectrograms of original and reconstructed signals